Radio/mm/sub-mm Observations of AGB and RSG stars

Hans Olofsson

Dept. of Earth and Space Sciences, Chalmers

Outline

I will cover the following topics:

The central stars

Chemistry:

- Spectral scans
- Source comparisons
- More elaborate modelling
- H_2O in CSEs (not covered)
- Large samples

Isotopes

Mass loss:

- Mass-loss rate
- M_{lost} and large-scale structure

Polarisation (not covered)
Binarity (not covered)

I will summarise the most recent findings in those areas where I think we will make huge progress through the use of ALMA.

Masers will be covered elsewhere

The central stars

How do they look like?

We are approaching the time when ALMA can resolve structures in the (radio) disks of red giants and supergiants.

This will put important constraints on the modelling of the stars themselves and the initial conditions for mass loss.

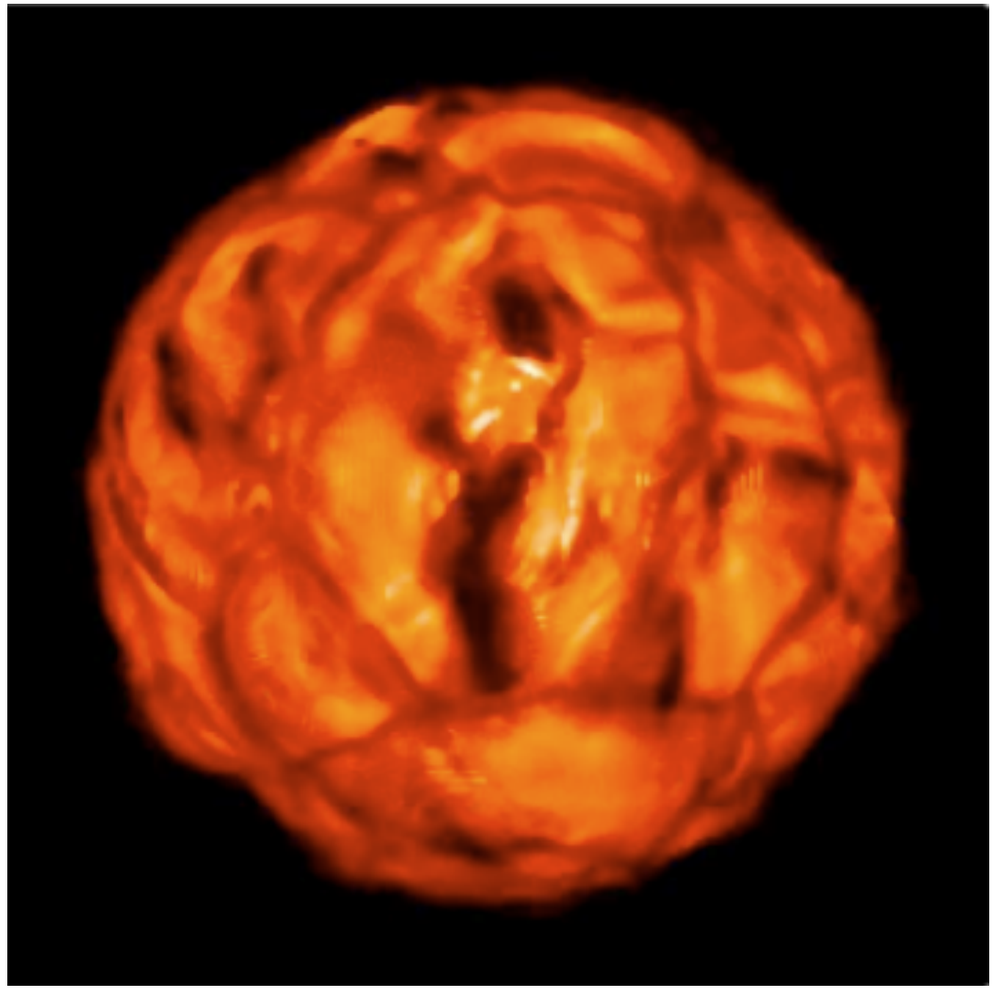

Do they look like this?

Important that the models produce radio images to compare observations with !!

Some simple estimates

Expected flux densities:

$$S_* \approx 1 \left[\frac{\nu}{115\,\mathrm{GHz}}\right]^2 \left[\frac{2000\,\mathrm{K}}{T}\right]^3 \left[\frac{L}{10^4\,L_\odot}\right] \left[\frac{1\,\mathrm{kpc}}{D}\right]^2 \ \mathrm{mJy}$$

$S_* \approx 80 \ \mathrm{mJy}$ for 230 GHz, 4000 $L_\odot$, 100 pc

$S_* \approx 20 \ \mathrm{mJy}$ for 230 GHz, 10^5 $L_\odot$, 1 kpc

Expected sizes:

$$\theta_* \approx 8 \left[\frac{L}{10^4\,L_\odot}\right]^{0.5} \left[\frac{2000\,\mathrm{K}}{T}\right]^2 \left[\frac{1\,\mathrm{kpc}}{D}\right] \ \mathrm{mas}$$

$\theta_* \approx 50 \ \mathrm{mas}$ for 4000 $L_\odot$, 100 pc

$\theta_* \approx 25 \ \mathrm{mas}$ for 10^5 $L_\odot$, 1 kpc

Pioneering work on the radio photospheres

- Reid & Menten, ApJ 476, 327, 1997;
  W Hya ≈80 mas at 22 GHz
- Reid & Menten, ApJ 671, 2068, 2007;
  o Ceti, R Leo, and W Hya ≈55 mas at 43 GHz
- Lim et al., Nature 392, 575, 1998
  α Ori ≈90 mas at 43 GHz

Sizes match well with the capacity of ALMA !!

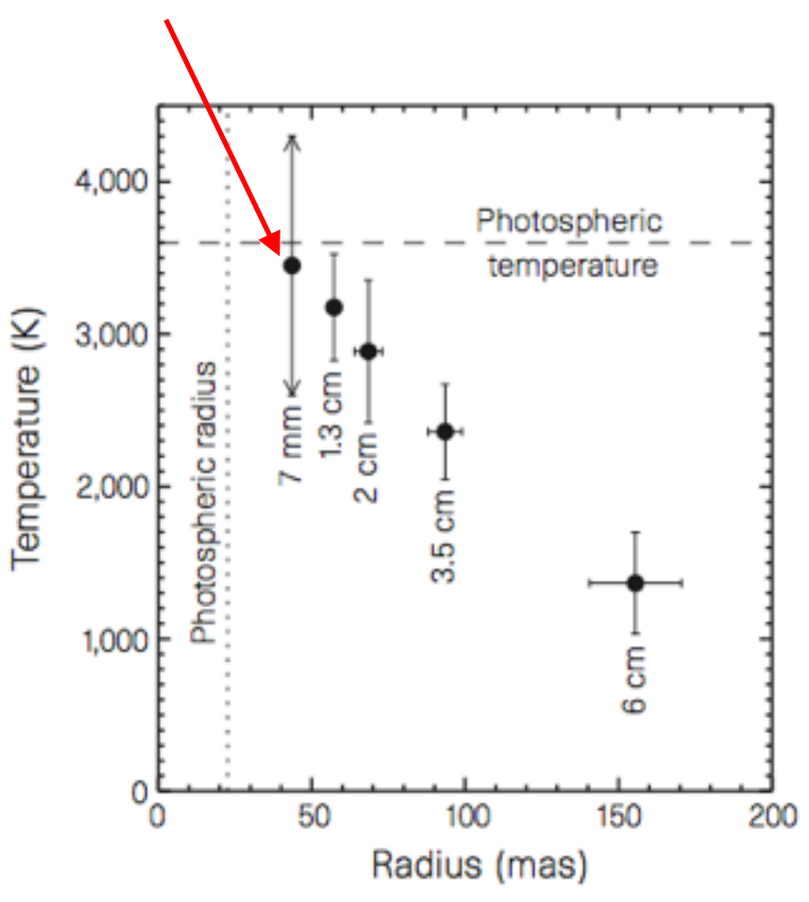

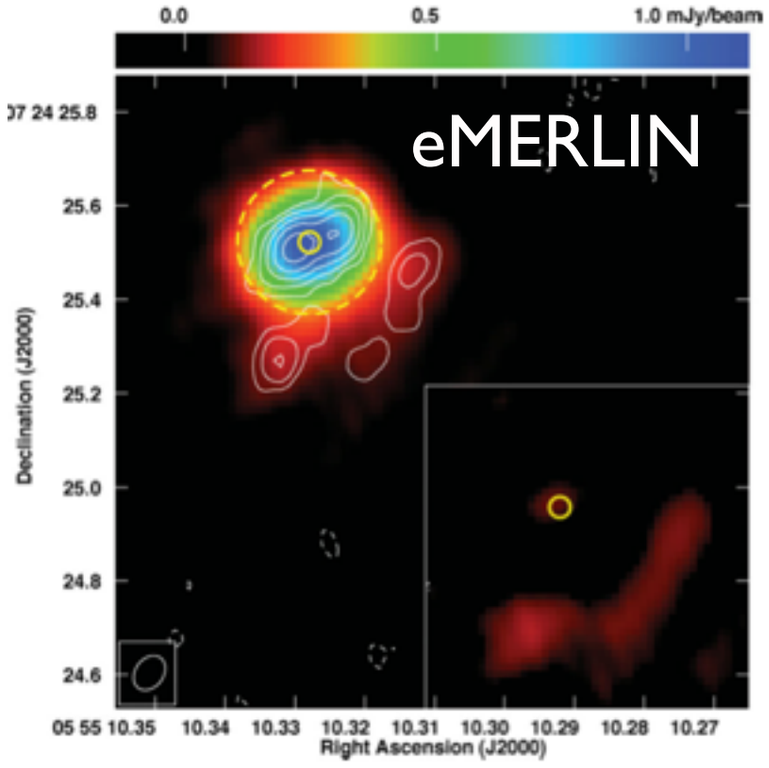

Richards et al.,
MNRAS 432, L61, 2013:

- α Ori, ≈230 mas at 6 GHz

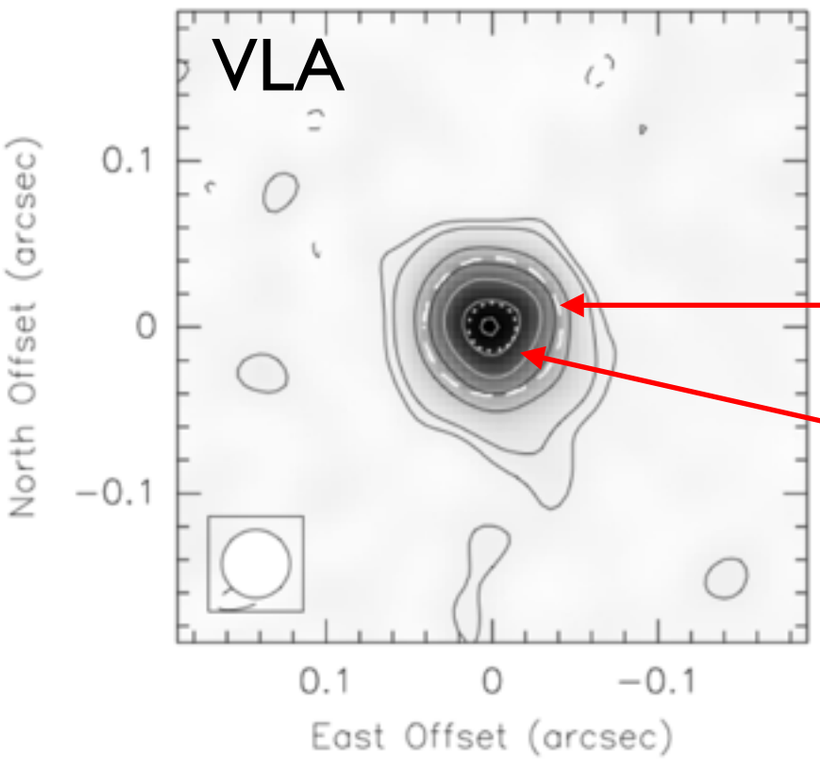

Menten et al., A&A 543, A73, 2012:

- CW Leo, ≈80 mas at 43 GHz

Radio photosphere at 43 GHz

Stellar photosphere

$R_* \approx$ 3.8 AU from estimated L and assumed T_{eff}

Vlemmings et al., A&A 577, L4, 2015:

- o Ceti, ≈40 mas (R* ≈ 1.8 AU) at 94 and 228 GHz
- A bright hotspot T_b ~ 10000 K, on the stellar disk of Mira A

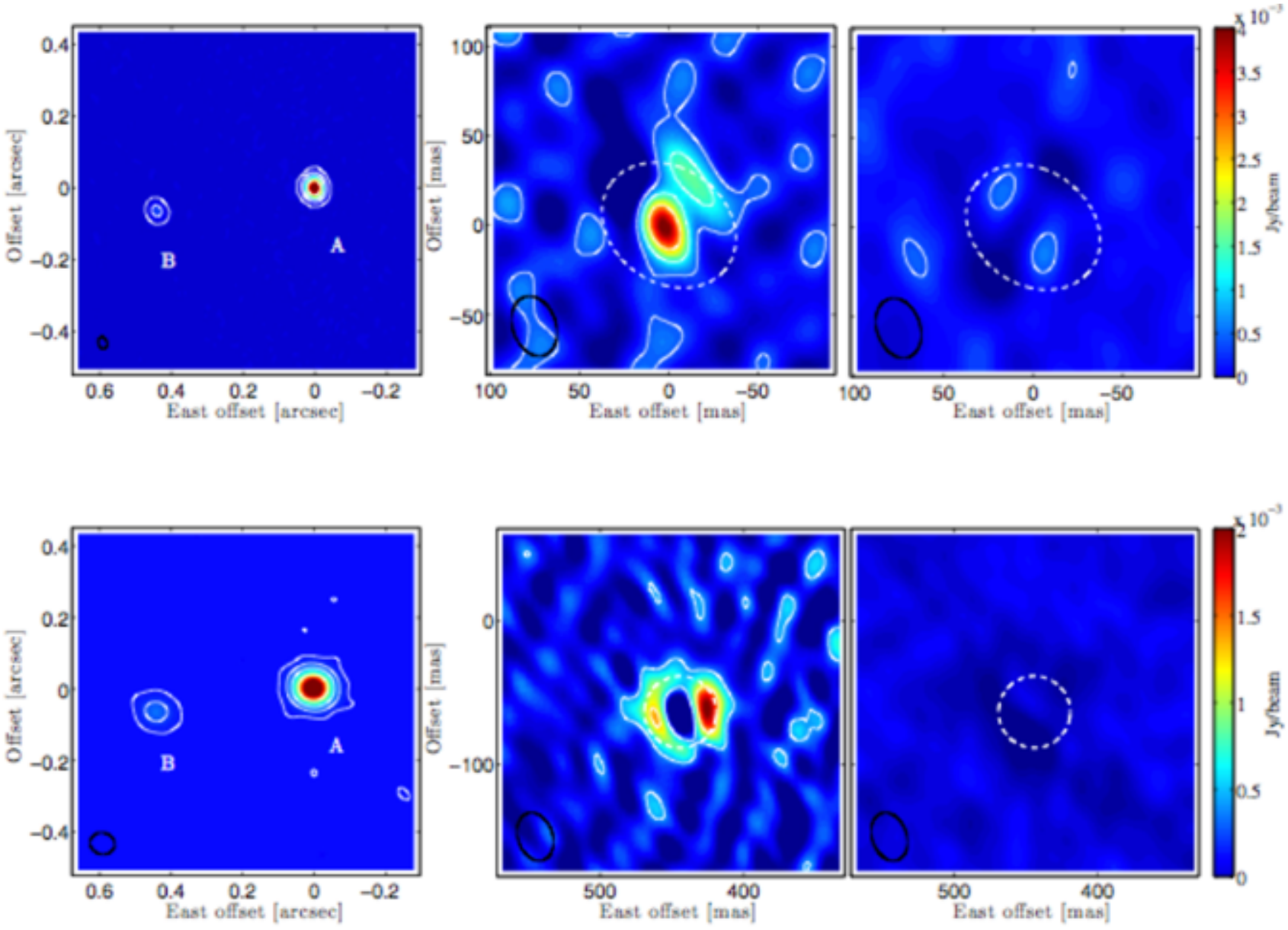

ALMA Band 6

ALMA Band 3

Chemistry: overview

Table 1: Molecules detected in AGB CSEs

2-atoms:	AlCl	CP	NaCl	SiO
	AlF	CS	OH	SiS
	C_2	ClH	PN	SO
	CO	FH	SiC	
	CN	KCl	SiN	
3-atoms:	AlNC	FeCN	HNC	SiC_2
	C_3	HCN	KCN	SiCN
	C_2H	HCP	MgCN	SiCSi
	C_2S	H_2O	MgNC	SiNC
	CO_2	H_2S	NaCN	SO_2
4-atoms:	ℓ-C_3H	C_2H_2	HMgNC	PH_3
	C_3N	HC_2N	MgC_2H (?)	SiC_3
	C_3O	H_2CO	NC_2P (?)	
	C_3S	H_2CS	NH_3	
5-atoms:	C_5	c-C_3H_2	CH_2NH	H_2C_3
	C_4H	CH_2CN	HC_3N	HNC_3
	C_4Si	CH_4	HC_2NC	SiH_4
6-atoms:	C_5H	C_5S	CH_3CN	H_2C_4
	C_5N	C_2H_4	HC_4N	SiH_3CN (?)
$\geq$*7-atoms:*	C_6H	CH_2CHCN	HC_7N	
	C_7H	CH_3CCH	HC_9N	
	C_8H	HC_5N	H_2C_6	
Ions:	C_4H^-	C_6H^-	C_8H^-	HCO^+
	CN^-	C_3N^-	C_5N^-	

Number of detected molecules in AGB-CSEs: 85 + 3?

Number of detected molecules in RSG-CSEs: ≈25

To a first approximation the difference is due to the RSGs being O-rich

(Imaging) Spectral Scans

The importance of unbiased spectral scans for understanding circumstellar chemistry must be emphasized !!

Cernicharo et al. (2010)
A&A 521, L8:
HIFI spectral scan of CW Leo
488 - 1901 GHz
(555−637 GHz so far)

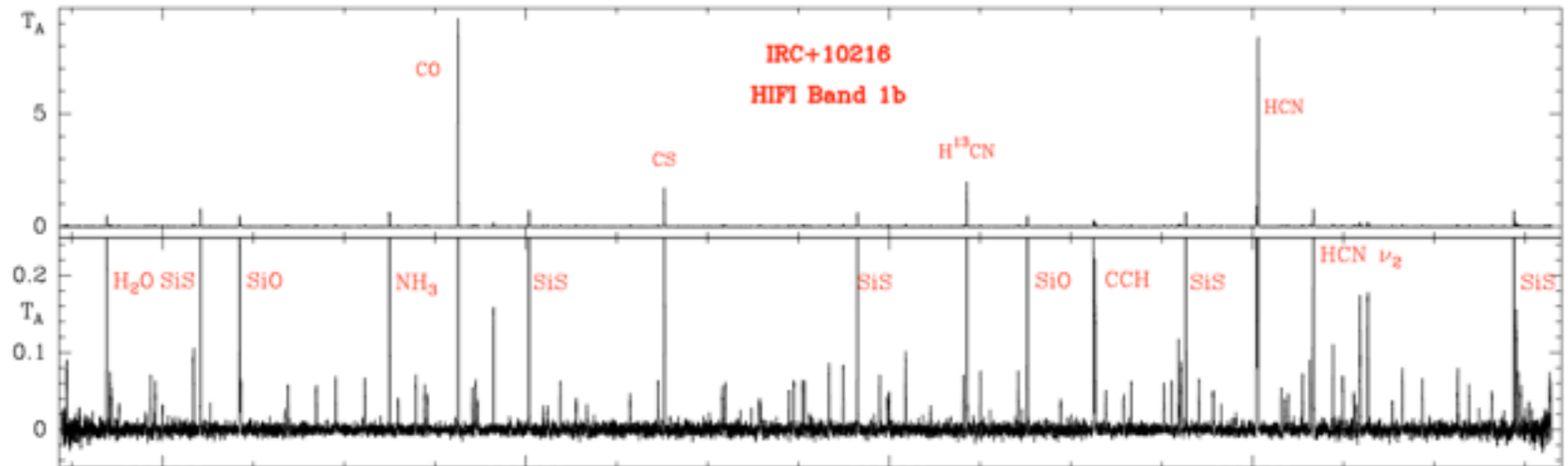

Patel et al. (2011):
ApJS 193, 17
SMA spectral scan of CW Leo
294 - 355 GHz.
442 lines were detected;
149 are unassigned.

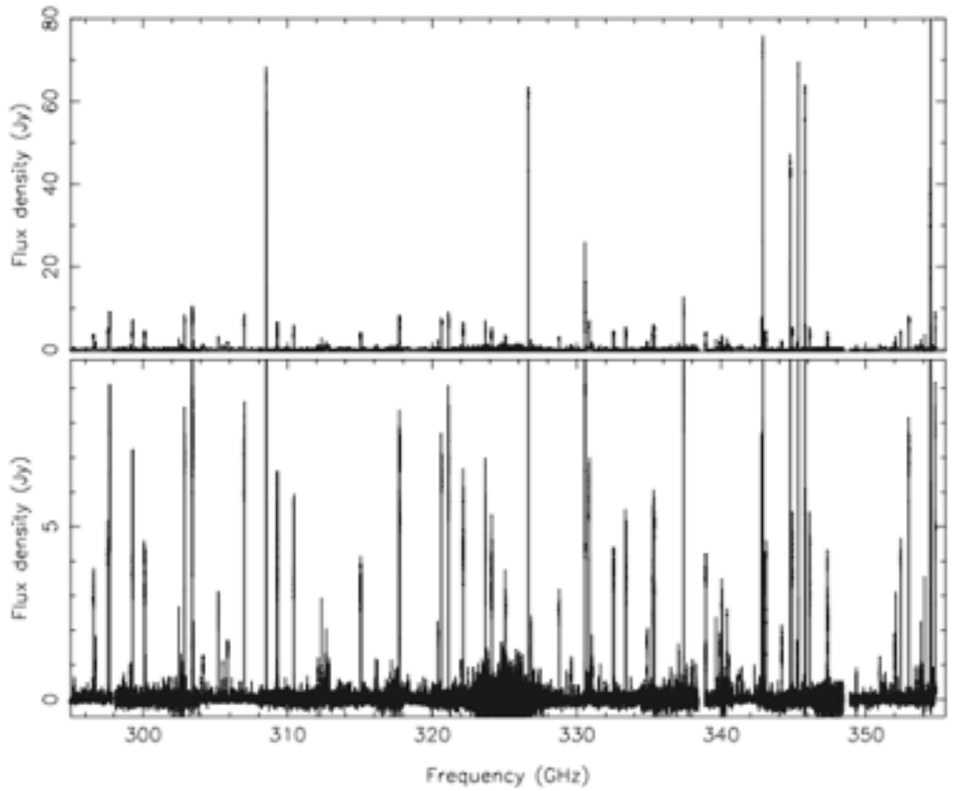

Figure 2. Overview of all the detected lines. Top and bottom panels show the same spectrum with different intensity scales.

Gong et al. (2015)
A&A 574, A56:
Effelsberg 100m telescope spectral scan of CW Leo, 17.8 - 26.3 GHz.
78 lines were detected;
12 are unassigned.

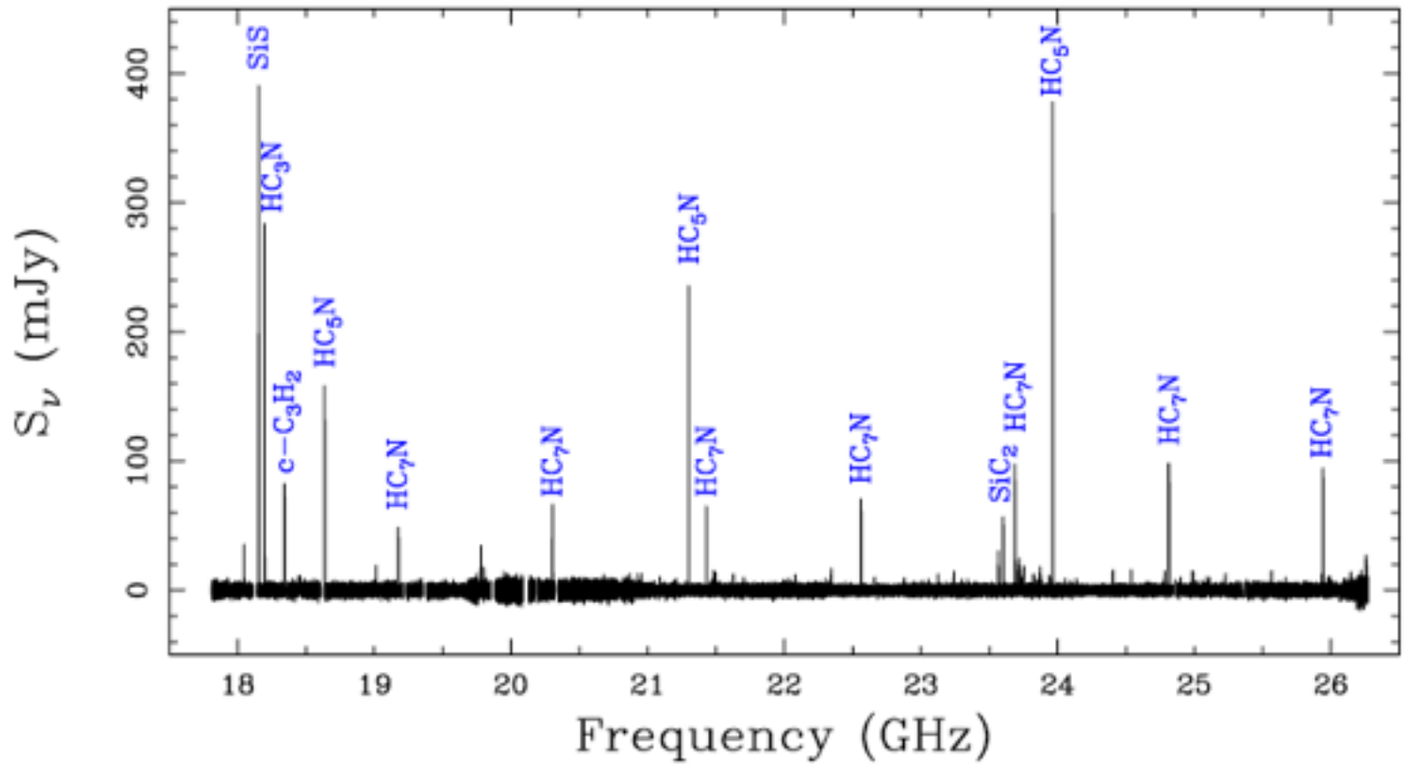

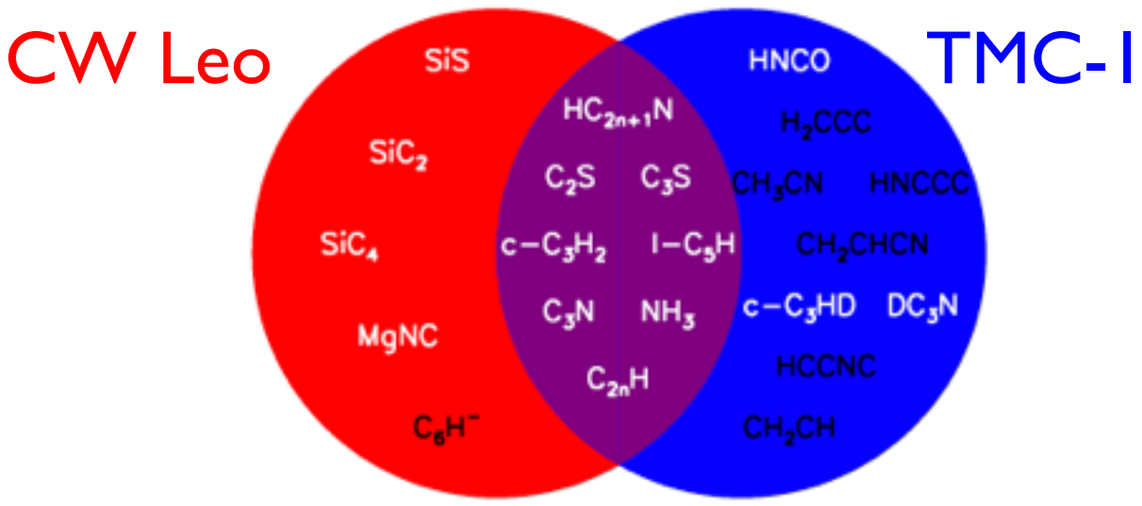

Fig. 5. Schematic diagram of detected molecules in the same $\lambda \sim 1.3$ cm spectral range toward IRC +10216 and TMC-1. Molecules in the red, blue, and purple regions indicate that they are detected in IRC +10216, TMC-1, and both sources, respectively. The molecules in black indicate that they have been seen in both sources but are not detected toward the other source in the $\lambda \sim 1.3$ cm spectral range (see Sect. 4.5).

At these frequencies it is possible to compare with dark cloud chemistry !!

Cernicharo et al. (2013)
ApJ 778, L25:
ALMA "spectral scan" of CW Leo
? - ? GHz

IRAM 30m

ALMA

Note:
the large effects of
resolved out flux !!
&
the large number of
U-lines !!

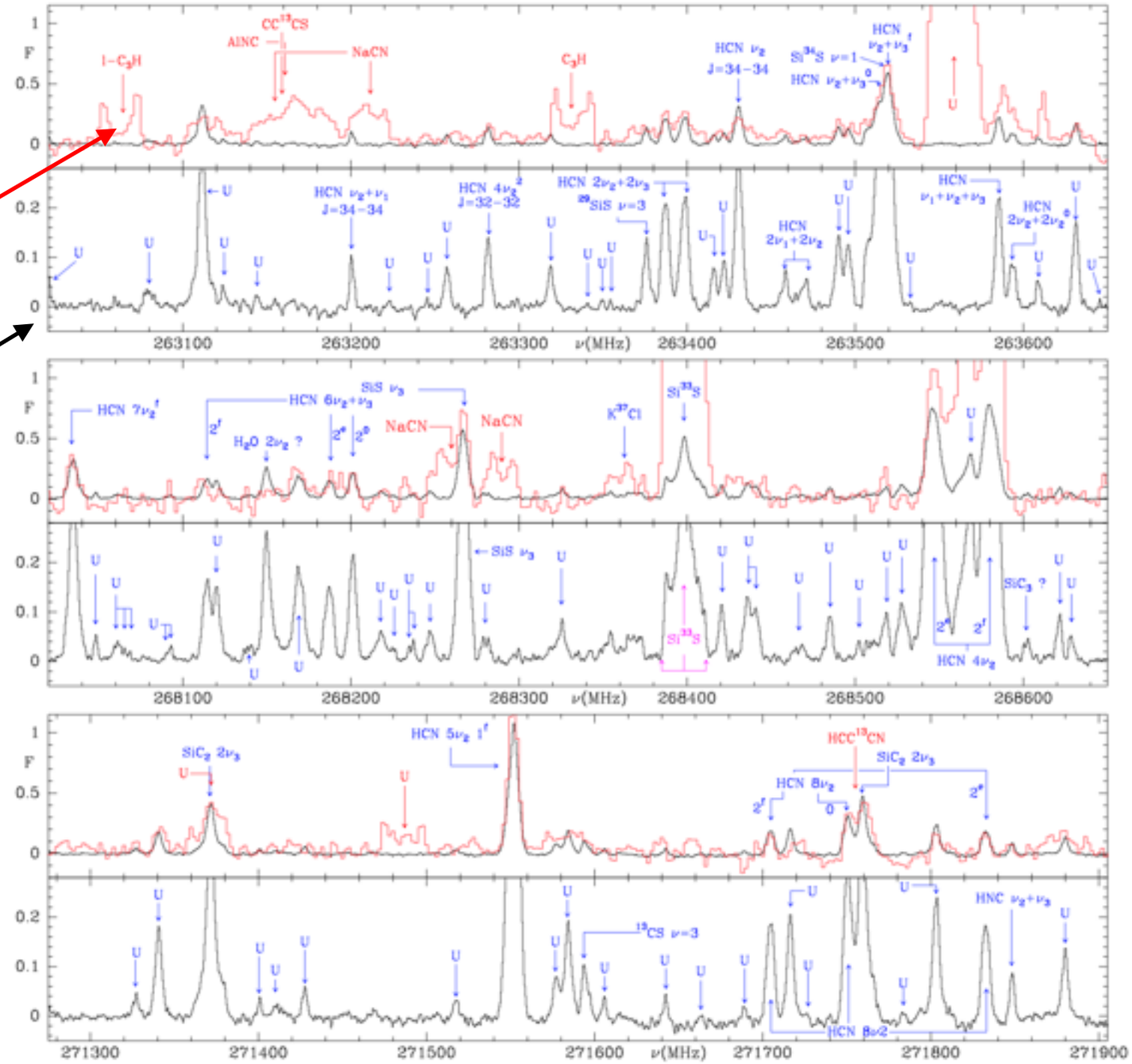

Figure 1. ALMA spectrum (black) of IRC+10216 in three selected frequency ranges of the 20 GHz bandwidth covered by our data. For each selected frequency the ALMA spectrum is compared to the data obtained with the 30-m IRAM telescope (red) at the same frequency (Cernicharo et al. 2011). Intensity scale is in units of Jy Beam^{-1}. Spectral resolution is ~1 MHz for both datasets. The bottom panel of each selected frequency shows a close-up view of the ALMA data. Interestingly, a forest of narrow and unidentified lines are evidenced thanks to the extreme sensitivity, and much higher angular resolution, of ALMA. Note the good calibration agreement for lines spatially unresolved by both instruments. Labels in red correspond to lines detected with the 30-m telescope and filtered by the interferometer.

Source comparisons

Fortunately it is not only CW Leo !!

Tenenbaum et al. (2010)
ApJS 190, 348; ApJ 720, L102:
ARO spectral scans of
CW Leo and VY CMa,
215 - 289 GHz.
CW Leo: 717 lines were detected;
126 are unassigned
VY CMa: 130 lines were detected;
14 are unassigned.

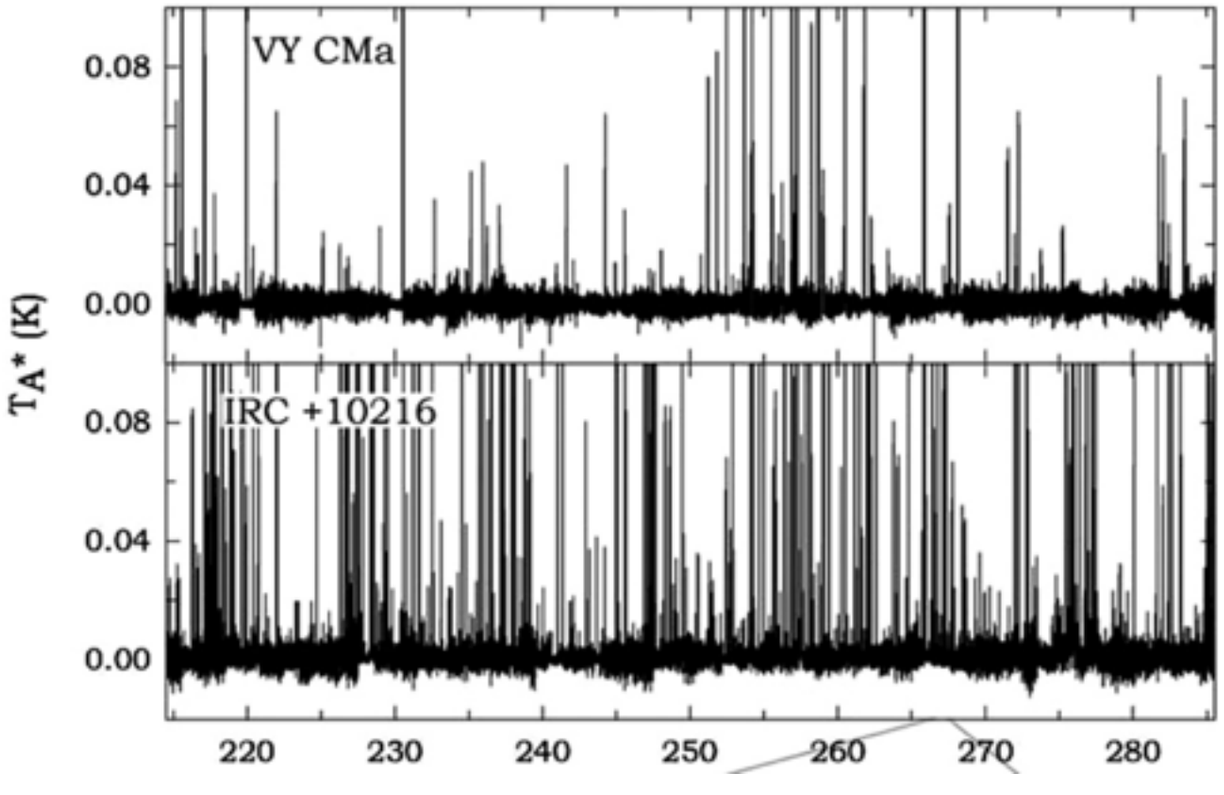

Species Observed in this Survey Toward IRC +10216 and VY CMa[a]

IRC +10216 C-rich		VY CMa O-rich	
Molecule	No. of lines	Molecule	No. of lines
CO	5	**CO**	2
SiO	6	**SiO**	12
SiS	47	**SiS**	21
CS	10	**CS**	1
CN	16	**CN**	3
HCN	17	**HCN**	3
HNC	3	**HNC**	1
NaCl	11	**NaCl**	11
PN	2	**PN**	2
HCO^+	1	**HCO^+**	1
PH_3[b]	1	NS	2
CH_2NH	9	PO[b]	6
CP	2	AlO[b]	2
SiC	8	AlOH[b]	2
AlCl	10	SO	7
KCl	9	H_2O	3
AlF	2	SO_2	36
SiN	4	H_2S	1
HCP	2	U	14
SiC_2	138		
CCH	17		
NaCN	38		
l-C_3H	17		
c-C_3H	13		
C_3N	13		
H_2CO	3		
H_2CS	9		
HC_3N	13		
c-C_3H_2	16		
C_4H	124		
CH_3CN	24		
CH_3CCH	7		
U	123		
Total	720	Total	130

Notes.
[a] Bold font indicates molecules common to both sources.
[b] New species detected in this survey.

Zhang et al. (ApJ 691, 1660, 2009):
ARO/SMT spectral scan towards
RW LMi
131 – 160, 219 – 244, 252 – 268 GHz
74 lines were detected;
5 are unassigned

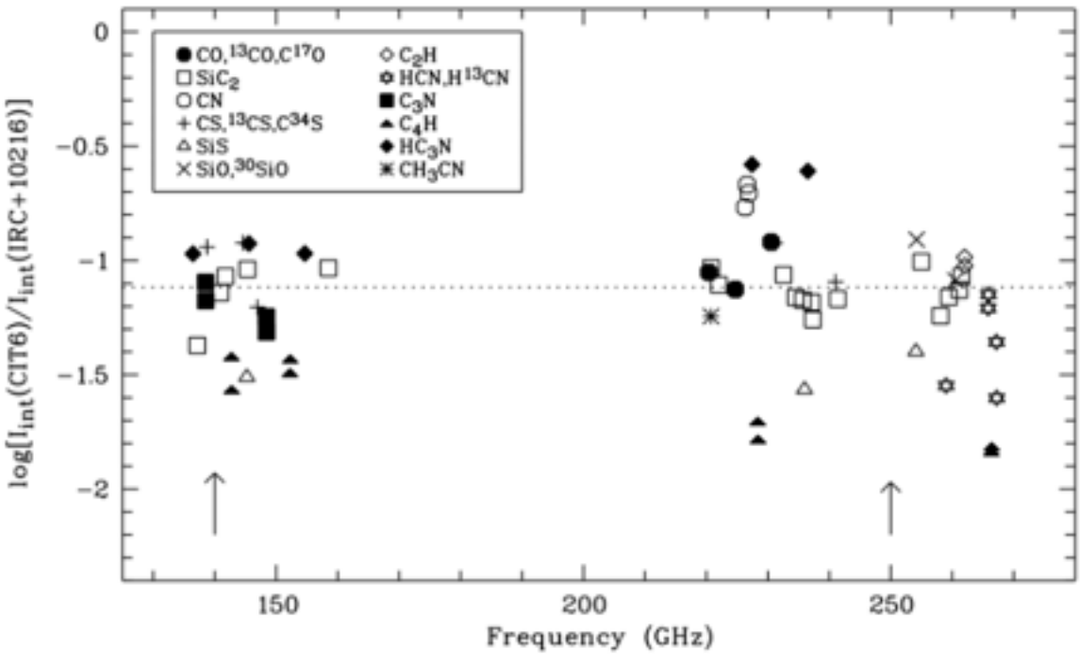

Enhanced emission from CN and HC_3N depleted emission from HCN, SiS, and C_4H in RW LMi (compared to CW Leo)

See also Chau et al. (ApJ 760, 66, 2012)

Zhang et al. (ApJ 700, 1262, 2009):
ARO/SMT spectral scan towards
AFGL3068
130 – 162, 220 – 268 GHz;
72 lines were detected;
3 are unassigned

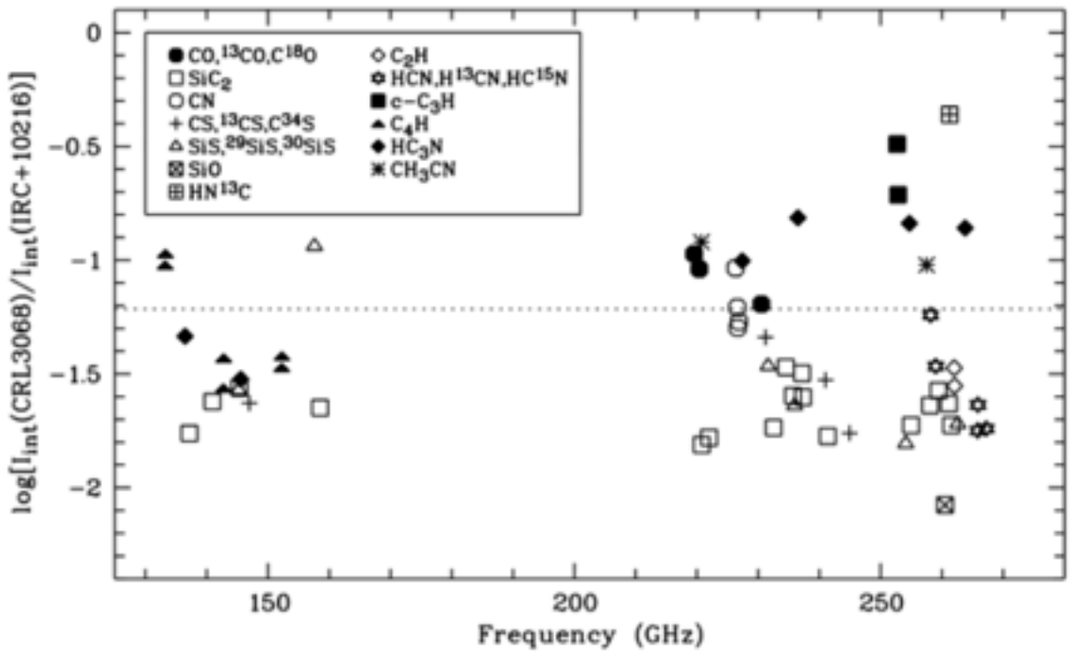

The chemical composition in AFGL3068 is somewhat different from that in CW Leo with a more extensive synthesis of cyclic and long-chain molecules in AFGL3068

Kaminski et al. (2013):
SMA spectral scan towards VY CMa
279 – 355 GHz
223 lines were detected;
19 different species

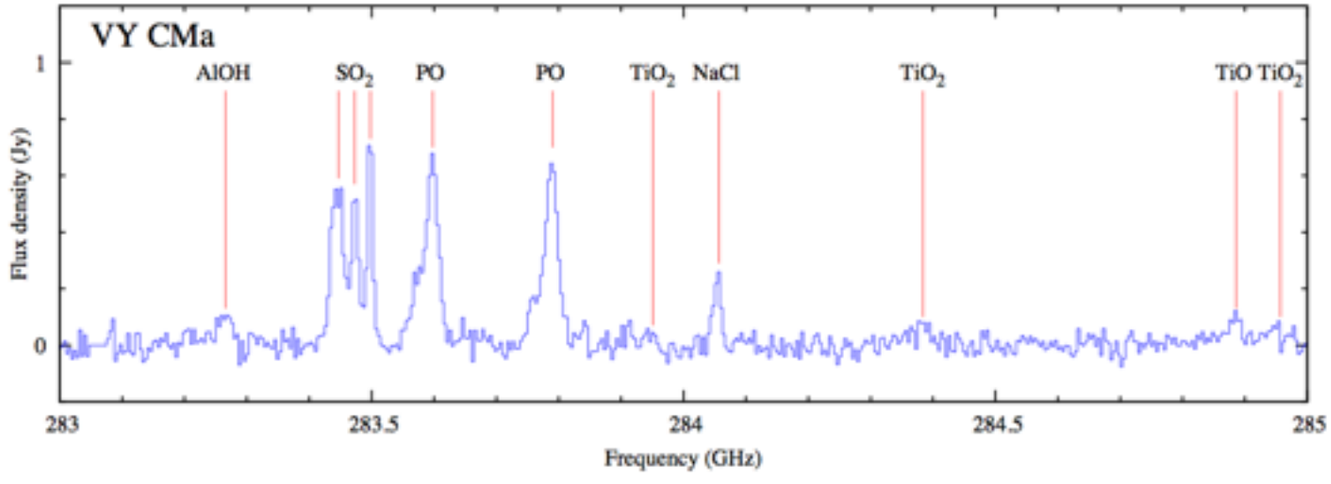

TiO, TiO_2, and AlCl detected for the first time in this source

De Beck et al. (in press)
followed this up in TiO_2 using ALMA

- Complex morphology
- Significant fraction of TiO_2 remains in the gas phase outside the dust-formation zone

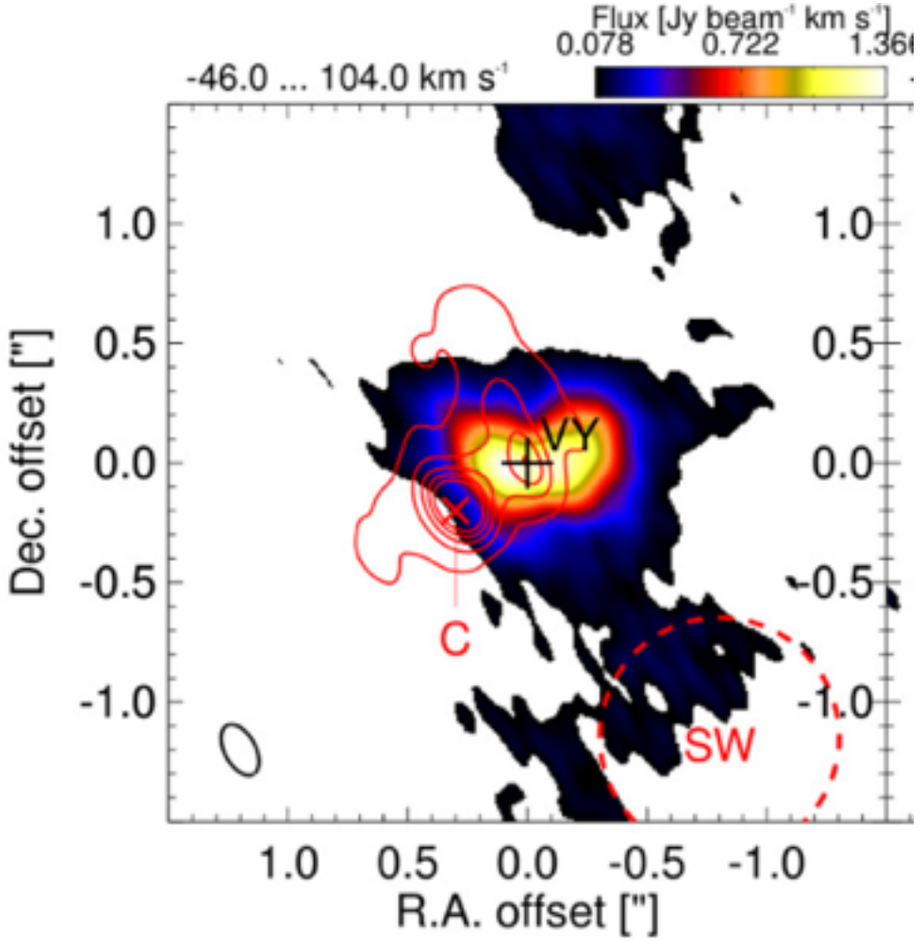

Chemistry: Detailed studies with more elaborate models

Detailed studies based on large number of lines

De Beck et al. (A&A 539, A108, 2012) presented IRAM, HIFI, and PACS observations of CO and C_2H

A detailed circumstellar model

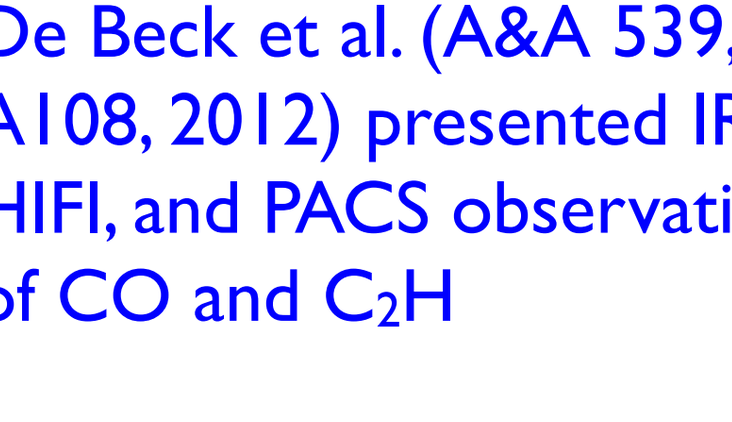

Fig. 5. Overview of the gas kinetic temperature and expansion velocity used in the radiative transfer model calculated with GASTRoNOoM. In the top panel, we indicate the exponents α from the $T_{kin}(r) \propto r^{\alpha}$-power laws used to describe the kinetic temperature, and the radial ranges they apply to. See Sect. 3.2.

CO

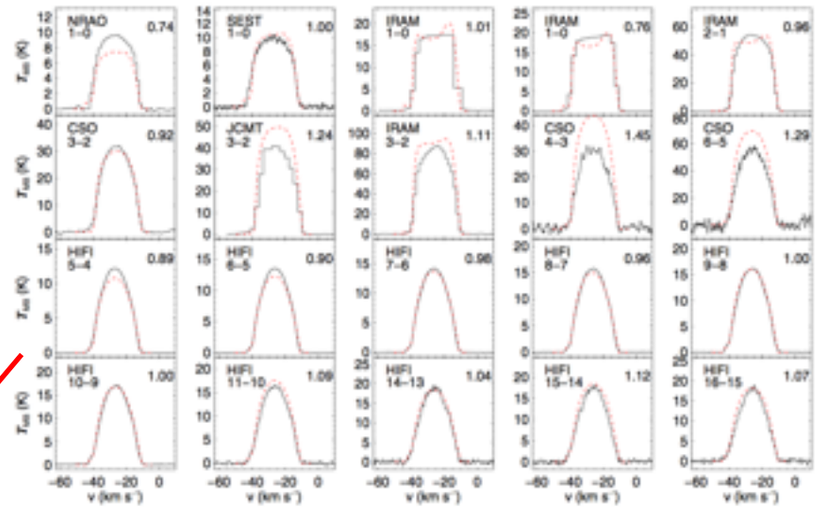

Fig. 6. Comparison of the observed ^{12}CO emission lines (*black histogram*), and the line profiles predicted by the GASTRoNOoM-model (*red dashed line*) with parameters as listed in Table 5. The line transitions $J - (J-1)$ and the telescopes with which they were observed are indicated in the *upper left corner of every panel*. The factor $I_{mb,model}/I_{mb,data}$ is given in the upper right corner of every panel.

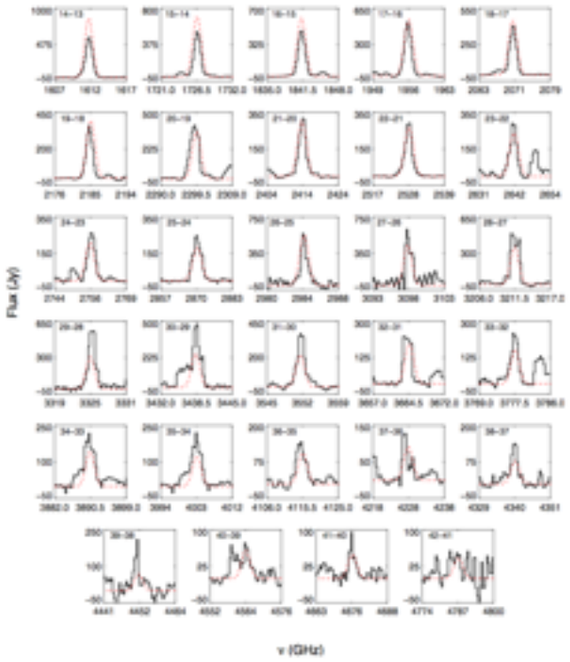

Fig. 7. Comparison of CO emission lines measured with PACS (*black histogram*) and the predicted line profiles (*red dotted line*). The transitions $J - (J-1)$ are labelled in the *top left corner* of each subpanel.

C_2H

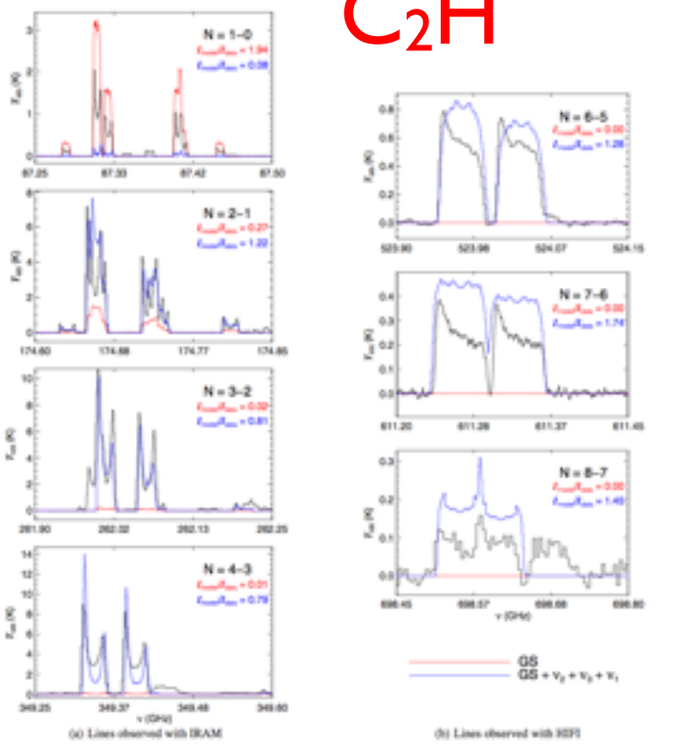

Fig. 13. Comparison of the measured C_2H spectra (*black histograms; see Sect. 2 and Fig. 1 for a description and for the identification of additional spectral features*) and GASTRoNOoM model predictions under NLTE conditions for the case where (*red*) only the ground state is included, and (*blue*) the ground state, and the three vibrational modes are taken into account. These predictions are based on the "enhanced" abundance profile shown in Fig. 10 and the $^2\Sigma$-approximation of C_2H. The transition $N - (N-1)$ and the ratio I_{mod}/I_{obs} are stated in the upper right corner of each panel, according to the colour code of the plots.

- The effect of density enhancements in the wind on the C_2H-abundance profile.
- The importance of radiative pumping to the vibrationally excited levels of C_2H.

Agundez et al. (A&A 543, A48, 2012) studied CS, SiO, SiS, NaCl, KCl, AlCl, AlF, and NaCN in CW Leo.

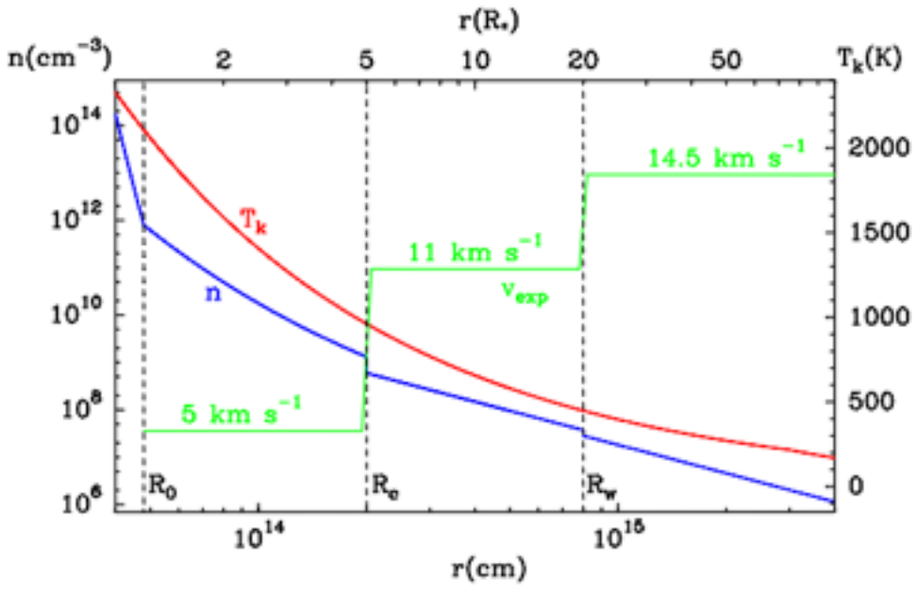

Fig. 1. Particle density n, gas kinetic temperature T_k, and expansion velocity v_{exp} as a function of radius in the inner layers of IRC +10216.

v=0 SiS v=5

J=19-18

J=5-4

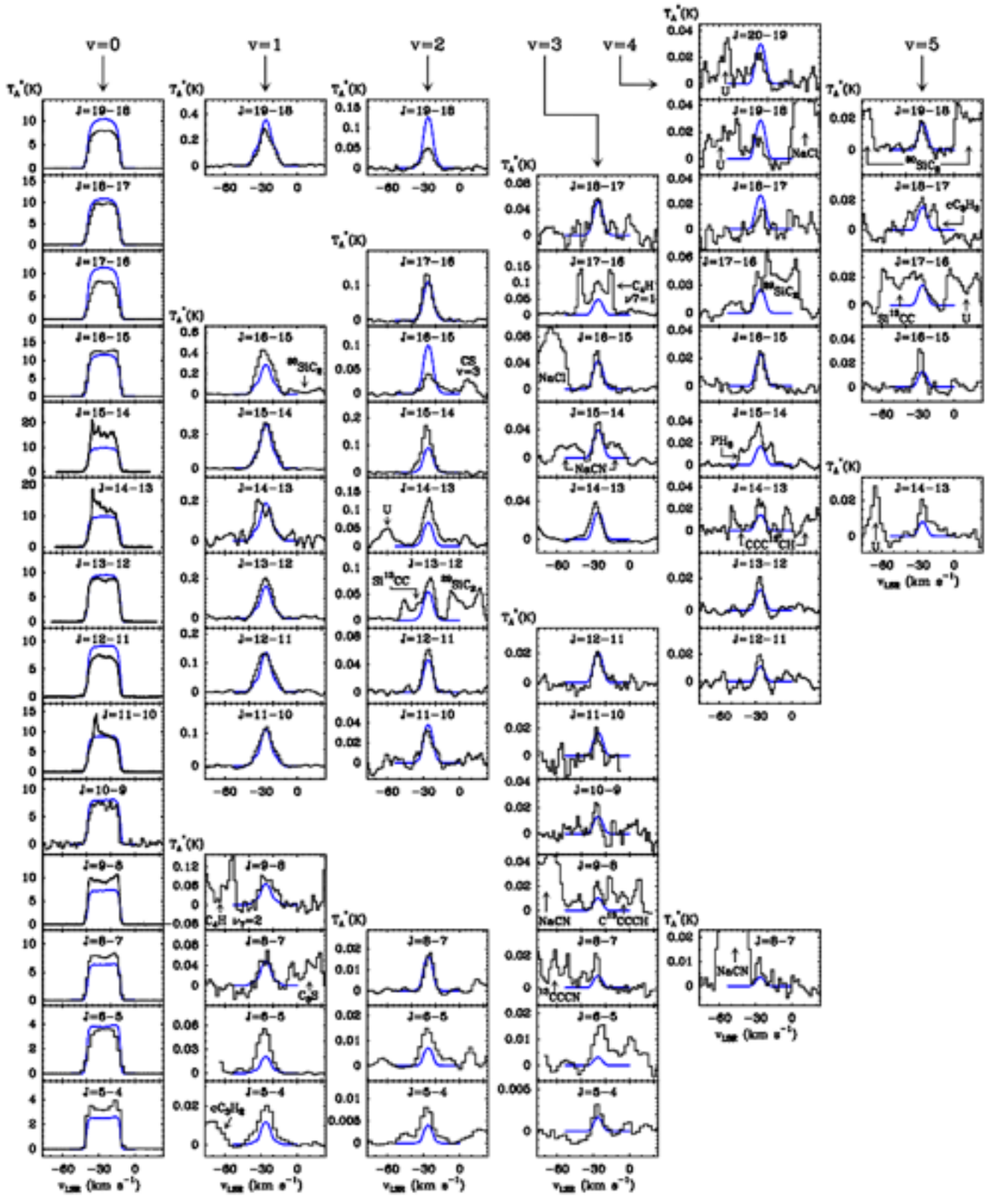

Fig. 5. Rotational lines of SiS in IRC +10216 as observed with the IRAM 30-m telescope (black histograms) and as calculated with the radiative transfer model (blue lines).

Detailed radial abundance distributions are derived:

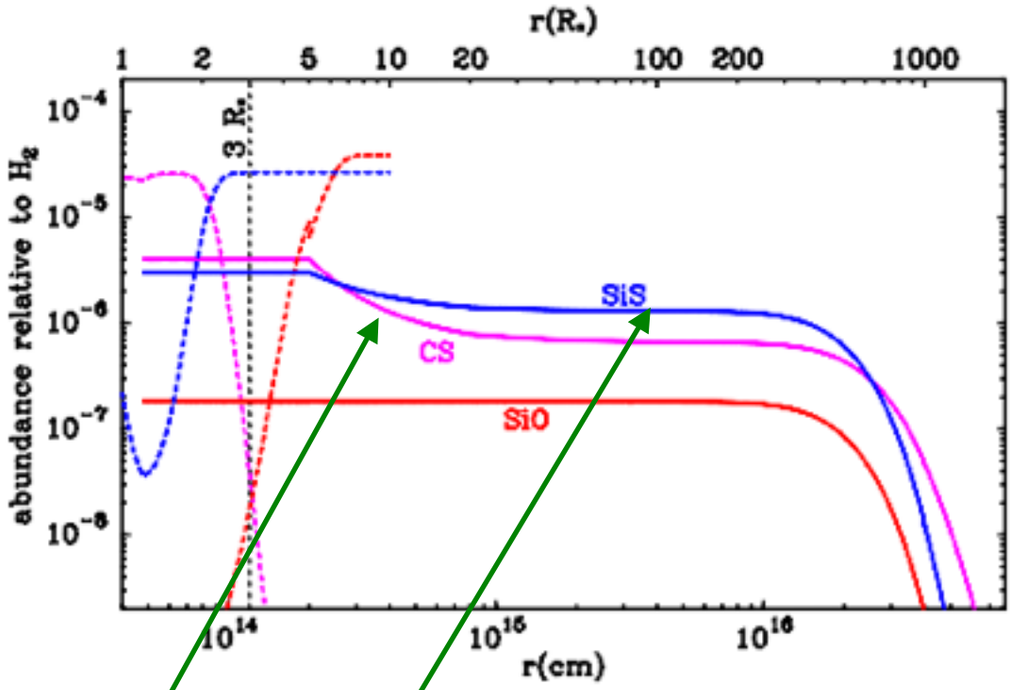

Fig. 12. Abundances of CS, SiO, and SiS in IRC +10216, as derived from the radiative transfer model (continuous lines) and as calculated through thermochemical equilibrium in the innermost regions of the envelope (dashed lines). A vertical dashed line indicates the outer boundary where thermochemical equilibrium is valid (~3 R_*).

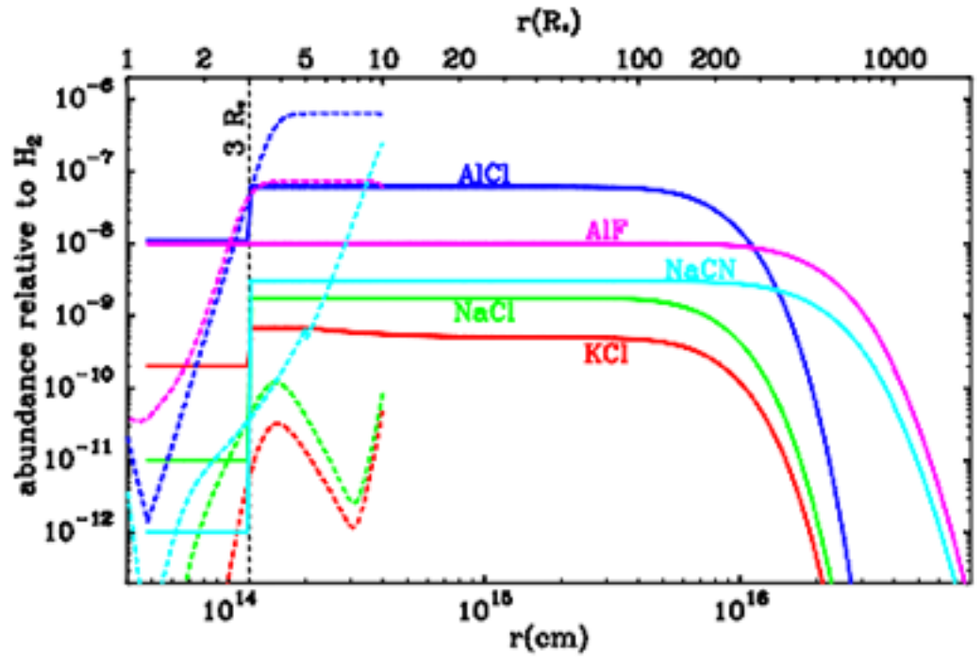

Fig. 13. Abundances of NaCl, KCl, AlCl (including ^{35}Cl and ^{37}Cl), AlF, and NaCN in IRC +10216, as derived from the radiative transfer model (continuous lines) and as calculated through thermochemical equilibrium in the innermost regions of the envelope (dashed lines). A vertical dashed line indicates the outer boundary where thermochemical equilibrium is valid (~3 R_*).

- CS and SiS have significant lower abundances in the outer envelope, which implies that they actively contribute to the formation of dust.
- The amount of sulfur and silicon in gas phase molecules is only 27% for S and 5.6% for Si. This implies that these elements have already condensed onto grains, most likely in the form of MgS and SiC.
- Metal-bearing molecules lock up a relatively small fraction of metals. The results indicate that NaCl, KCl, AlCl, AlF, and NaCN, despite their refractory character, are not significantly depleted in the cold outer layers.

Daniel et al. (A&A 542, A37, 2012) presented a study of HNC in CW Leo based on IRAM and HIFI observations

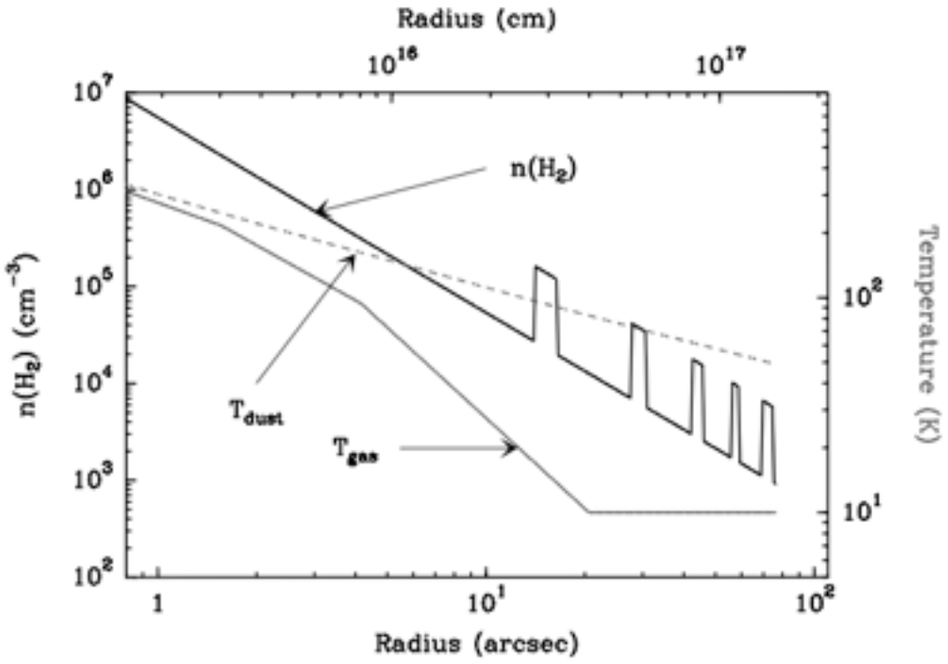

Fig. 2. Physical parameters (i.e. dust and gas temperatures, H_2 volume density) used in the present work to describe the circumstellar envelope. Density-enhanced shells are introduced in the current modeling as can be seen in the H_2 volume density curve. The first shell is located at 15″ and we assume an intershell distance of 12″, the shells being 2″ wide.

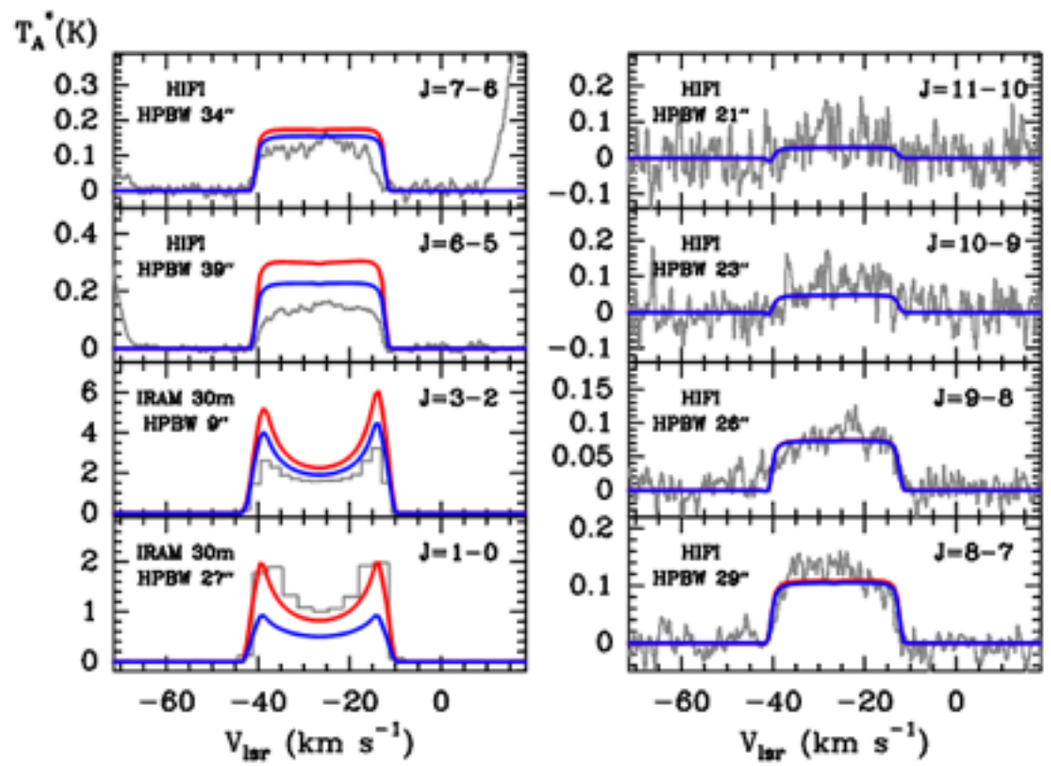

Fig. 9. HNC line profile for the model with density-enhanced shells (red) and for the model without shells (blue).

- The presence of HNC is consistent with formation from the precursor ion $HCNH^+$.
- Radiative pumping through 21 μm photons to the first excited state of the bending mode ν_2 plays a crucial role.

Followed up by observations of HNC from vibrationally excited states by Cernicharo et al. (ApJ 778, L25, 2013) using ALMA.

Cernicharo et al. (A&A 518, L136, 2010) & Agundez et al. (A&A 533, L6, 2011):
The abundances relative to H_2 derived for HF and HCl in CW Leo, 8×10^{-9} and 10^{-7} respectively, are *substantially lower than those predicted by thermochemical equilibrium*.

Agundez et al. (ApJ 790, L27, 2014):
The detection of PH_3 in CW Leo *challenges chemical models, none of which offer a satisfactory formation scenario*.

De Beck et al. (A&A 558, A132, 2013):
Detections of PN and PO in IK Tau suggest that PN and PO are the main carriers of phosphorus in the gas phase, with abundances possibly up to several 10^{-7}. *The current chemical models cannot account for this*.

Detailed studies of sources other than CW Leo

W Hya (O-rich)

Khouri et al. (A&A 561, A5, 2014
A&A 569, A76, 2014)

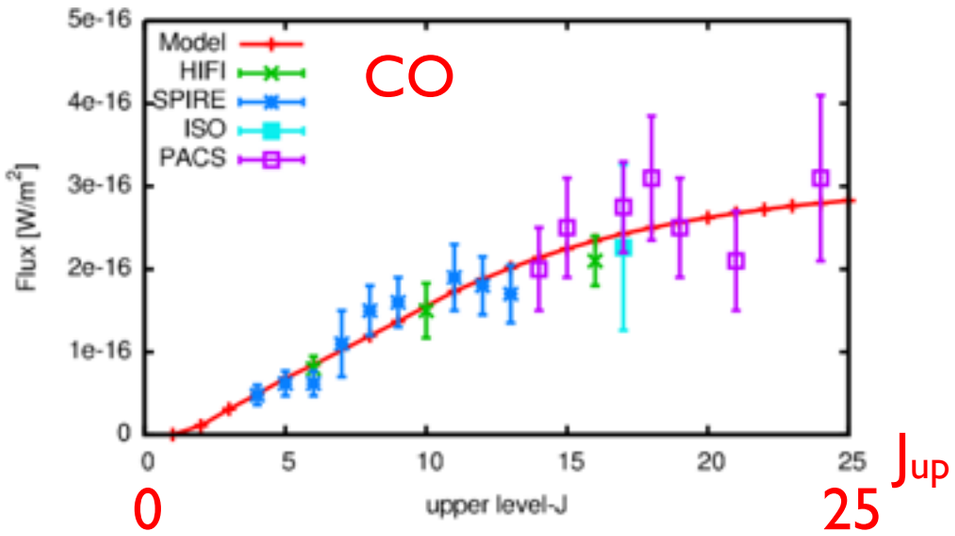

Fig. 6. Best grid model for the ^{12}CO observed integrated line fluxes, when considering the dissociation radius as given by Mamon et al. (1988). Transition ^{12}CO J = 16–15 observed by PACS and ISO is not used due to line blending (see Table 1).

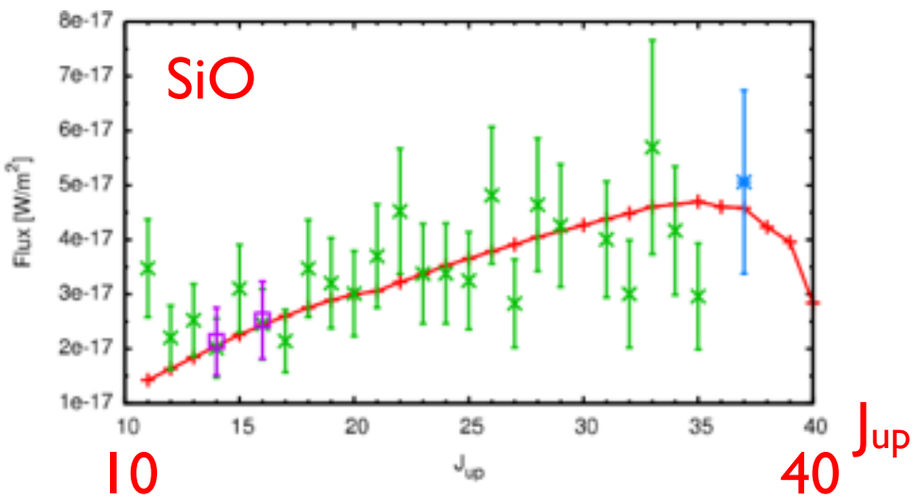

Fig. 10. Best model for the ^{28}SiO line emission (red line and crosses), with $f_o^{SiO} = 4 \times 10^{-5}$ and $f_{cond} = 0$, is compared to the line fluxes observed by SPIRE (green), PACS (blue) and HIFI (purple).

W Aql (S-star)

Danilovich et al. (A&A 569, A76, 2014)

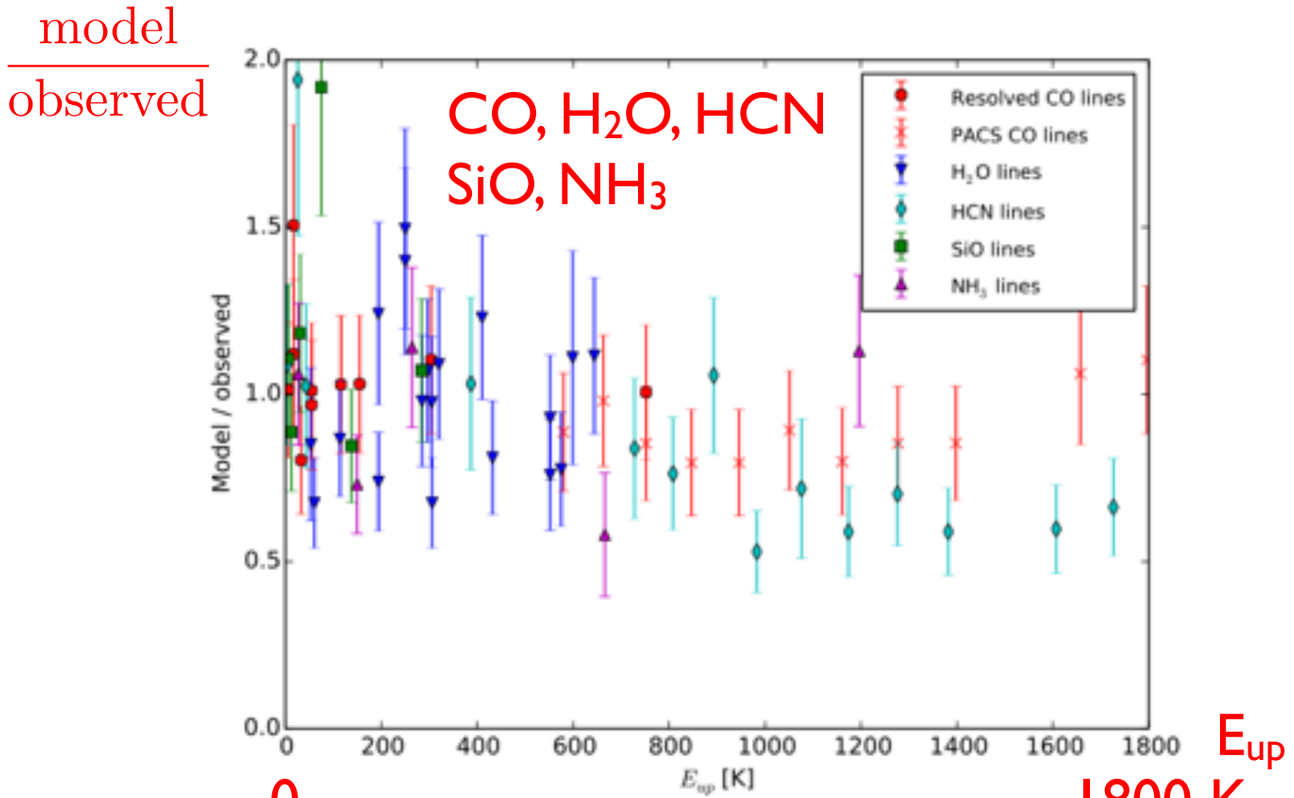

Fig. 8. Model line intensities (resolved lines) or total fluxes (PACS lines) divided by the corresponding observed intensities or fluxes. The horizontal axis gives the energy of the upper level of the transition. Model parameters are listed in Table 6.

One of the outcome is studies of the acceleration zone

Decin et al. (A&A 521, L14, 2010) used Herschel CO, H_2O, SiO, to derive velocity law for IK Tau.

$v_e(r)$

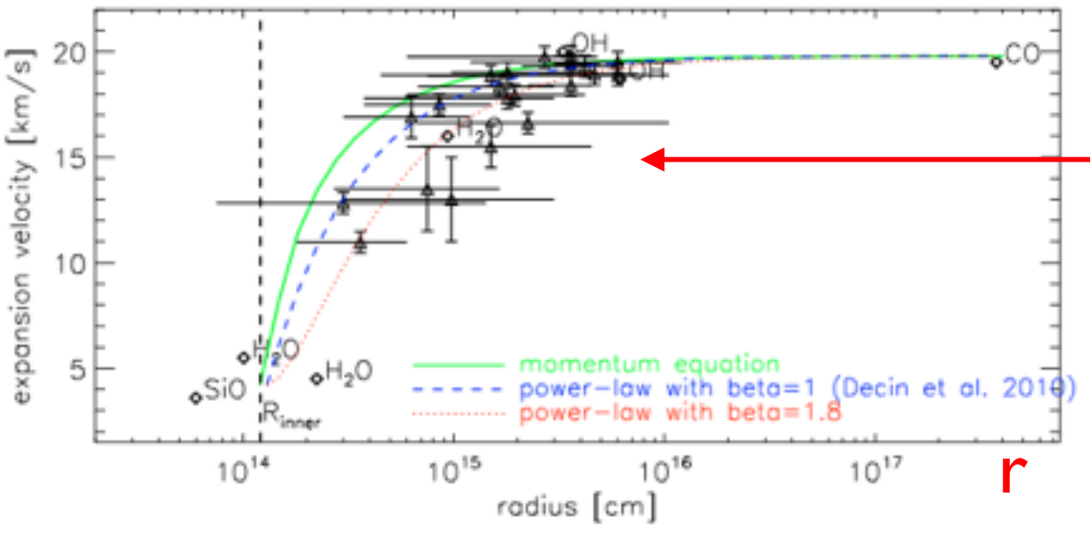

r

$$v(r) \simeq v_0 + (v_\infty - v_0)\left(1 - \frac{R_\star}{r}\right)^{\beta}$$

IK Tau β=1.8

W Hya β=5 (Khouri et al.)

W Aql β=2 (Danilovich et al.)

Any viable mass-loss mechanism must adhere to the behaviour in the acceleration zone !!

Chemistry: H_2O in CSEs

H_2O detected by SWAS and Odin in CW Leo, a consequence of vaporisation of icy objects.

Neufeld et al. (A&A 521, L5, 2010): H_2O in the C-star V Cyg,
Neufeld et al. (ApJ 717, L29, 2011): H_2O towards 8 C-stars using HIFI.

Decin et al. (Nature 467, 64, 2010) and Neufeld et al. (ApJ 727, L28, 2011) reported higher-energy H_2O lines in CW Leo using HIFI and PACS.

Can be explained only if H_2O is present in the warm inner CSE !!

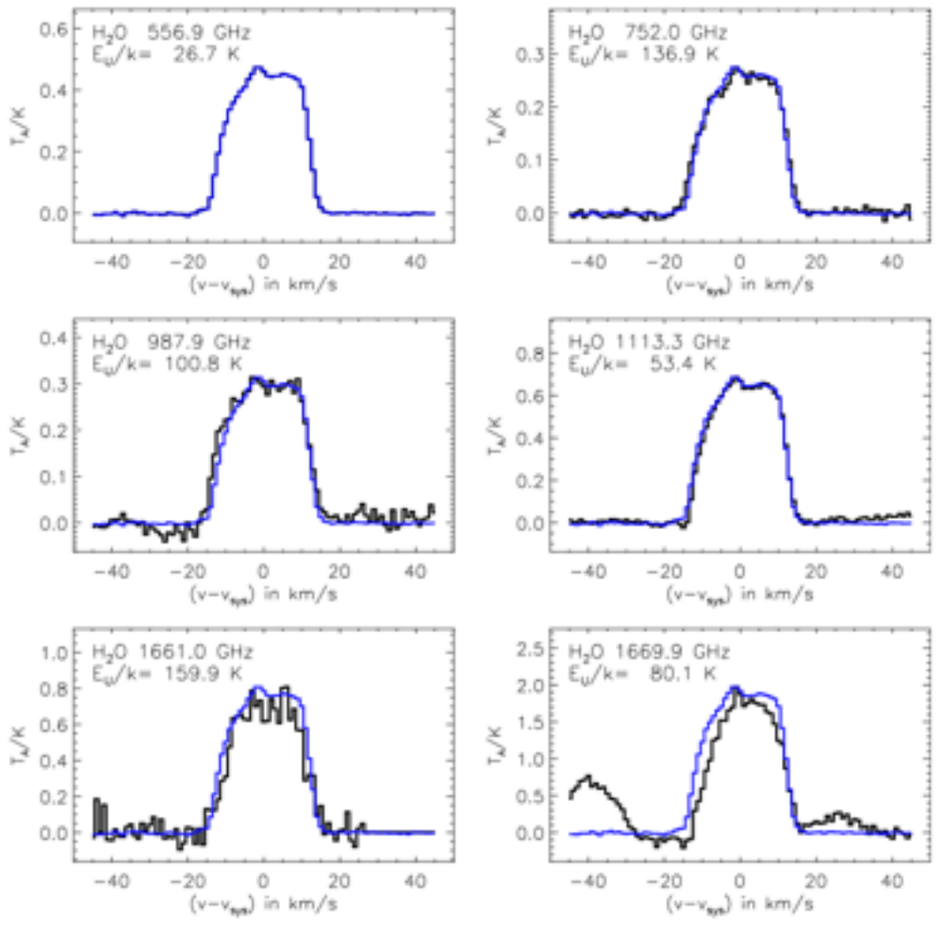

Agundez et al. (ApJ 724, L133, 2010) proposed a mechanism based on photodissociation in the inner CSE.

Cherchneff (A&A 526, L11, 2011) proposed a mechanism based on shock-induced chemistry in the upper atmosphere.

Neufeld et al. (ApJ 727, L28, 2011b; ApJ 767, L3, 2013): upper limits on the $H_2{}^{17}O/H_2{}^{16}O$ and $H_2{}^{18}O/H_2{}^{16}O$ isotopic abundances in CW Leo.

An upper limit of 1/470 on $H_2{}^{17}O/H_2{}^{16}O$, compared to the photospheric 1/840. Provides an important constraint on any model that invokes CO photodissociation as the source of O for H_2O production.

Of course there are detections of H_2O also in
M-stars: e.g., Maercker et al. (A&A 494, 243, 2009) and Justtanont et al. (A&A 537, A144, 2012)
S-stars: e.g., Schöier et al. (A&A 530, A83, 2011) and Danilovich et al. (A&A 569, A76, 2014)

Temporal variations in non-masing lines

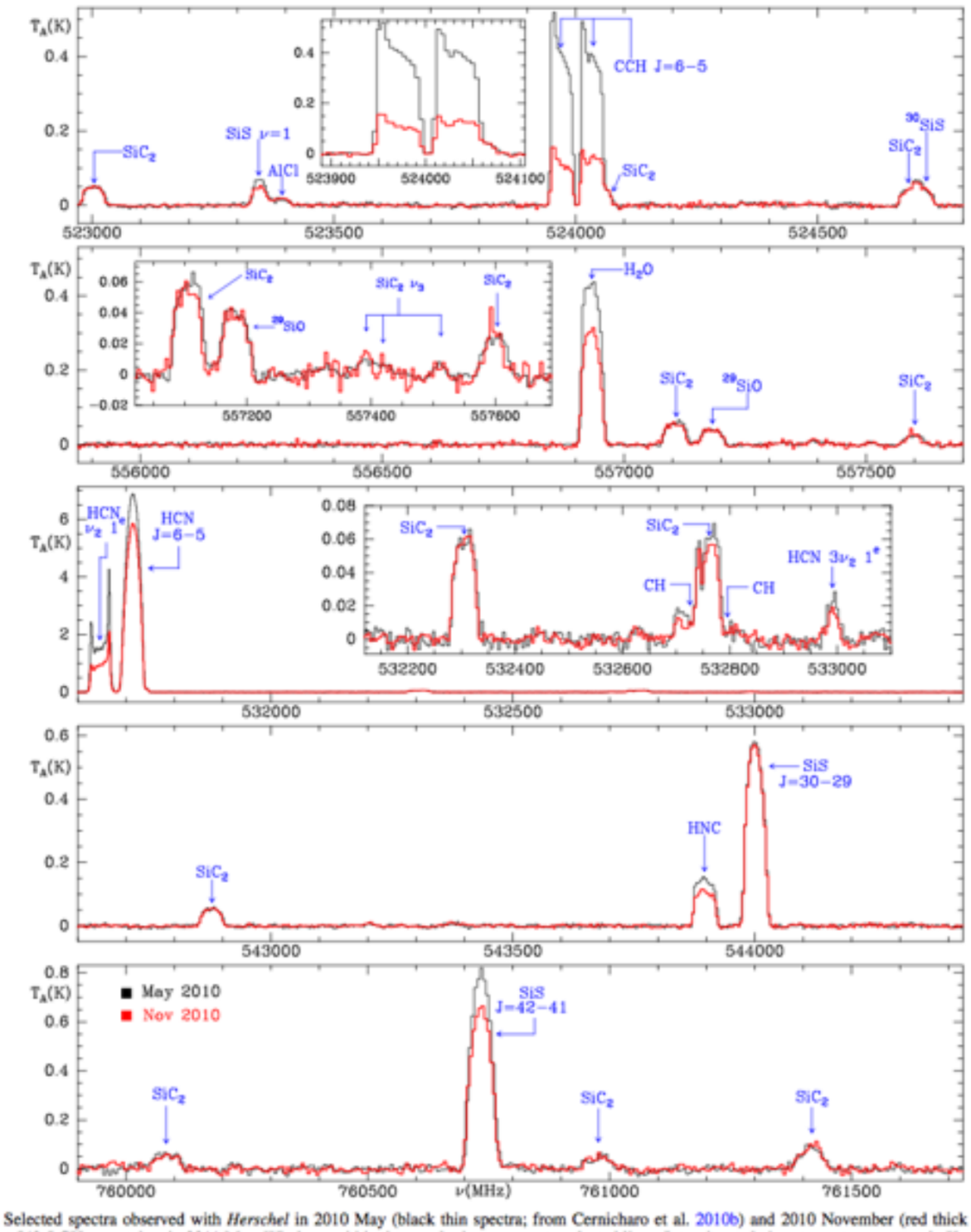

Figure 1. Selected spectra observed with *Herschel* in 2010 May (black thin spectra; from Cernicharo et al. 2010b) and 2010 November (red thick spectra). The spectrum at 543.5 GHz was taken in 2011 May. Windows within the panels show zooms to selected lines. Intensity scale is antenna temperature in K and abscissa is frequency in MHz.

Cernicharo et al. (ApJ 796, L21, 2014): Strong intensity variations in the high rotational lines of some abundant molecular species toward CW Leo.

CO, SiC_2: little variability

CS, SiO, SiS: ≈25% variation

HCN, HNC: 20%–50% variation

C_2H: strong variability

Chemistry: Large samples

Schöier et al., (A&A 473, 871, 2007; A&A 550, A78, 2013) & Ramstedt et al., (A&A 499, 515, 2009) studied samples of the order 20 M-, 20 S-, and 20 C-stars

These studies are still unique in terms of number of sources.

abundance

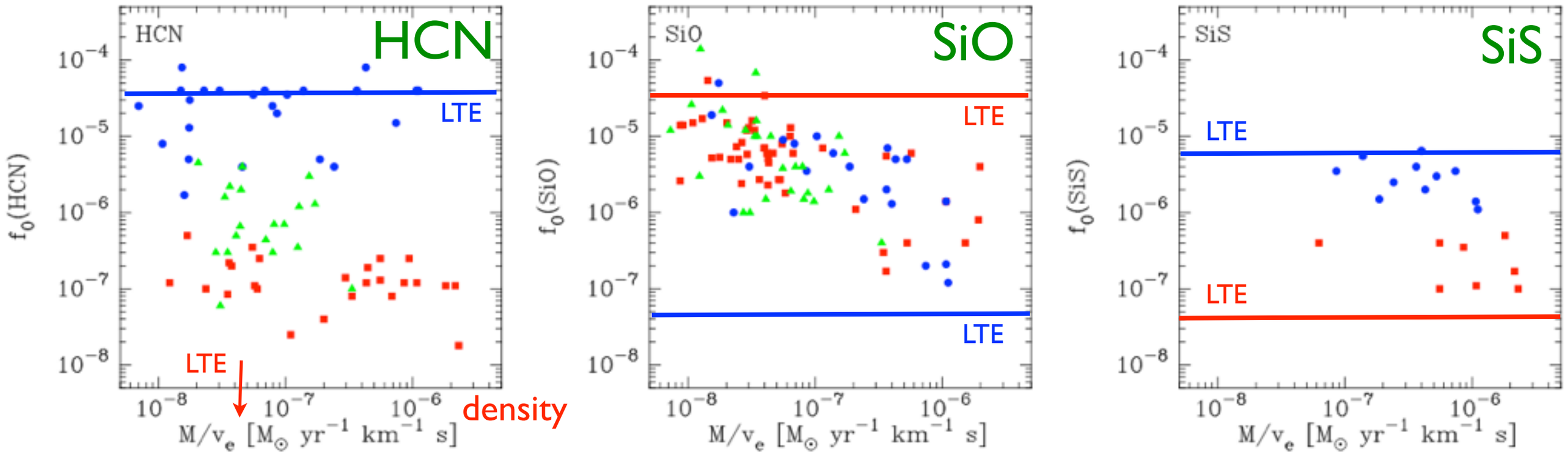

M-stars S-stars C-stars

Provide important constraints on chemical models !!

Isotopes

Isotope ratios are important tracers of stellar nucleosynthesis.

The problem is to convert I(^{n}XA) & I(^{m}YA) into [^{n}X] & [^{m}Y], i.e., molecular isotopologue ratios into elemental isotope ratios

A number of things need to be considered:

- Optical depths
- Isotope-different excitation (in some cases masering)
- Isotope-selective photodissociation
- Chemical fractionation

Circumstellar ^{12}C and ^{13}C

Ramstedt & Olofsson (A&A 566, A145, 2014) have presented an extensive study of circumstellar ^{12}CO and ^{13}CO

19 M- 17 S- 19 C-stars

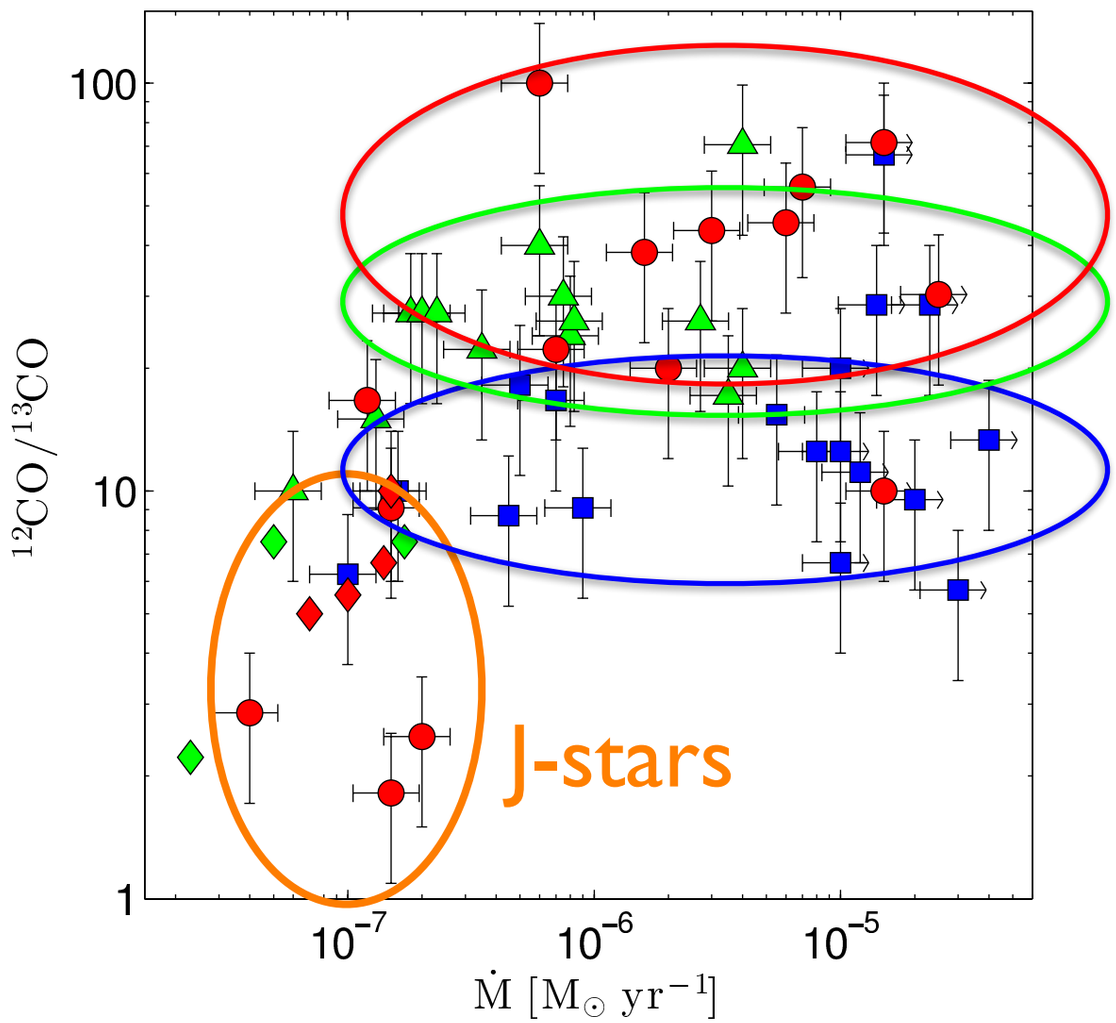

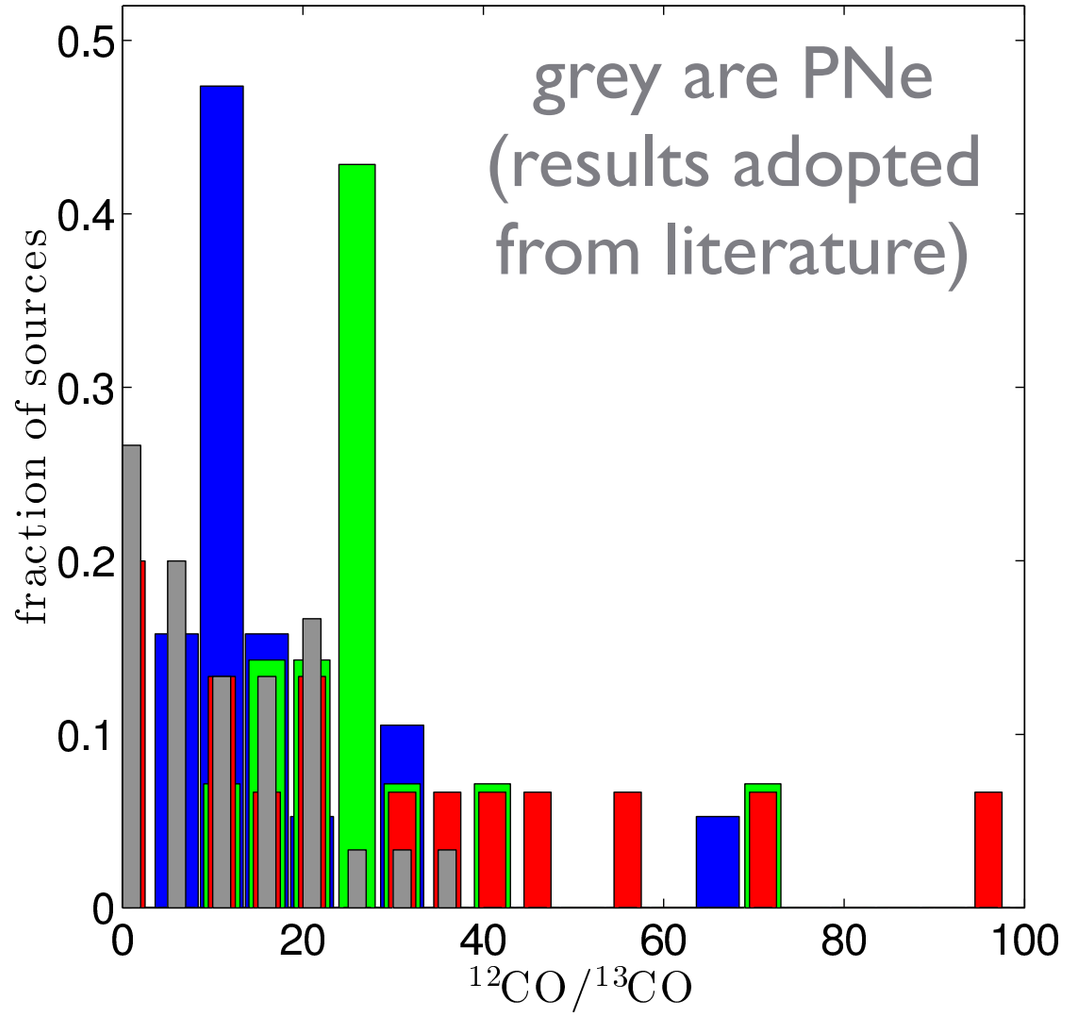

- The three chemical types have (on average) different $^{12}CO/^{13}CO$
- The J-stars are very different from the rest

Circumstellar ^{16}O, ^{17}O, and ^{18}O

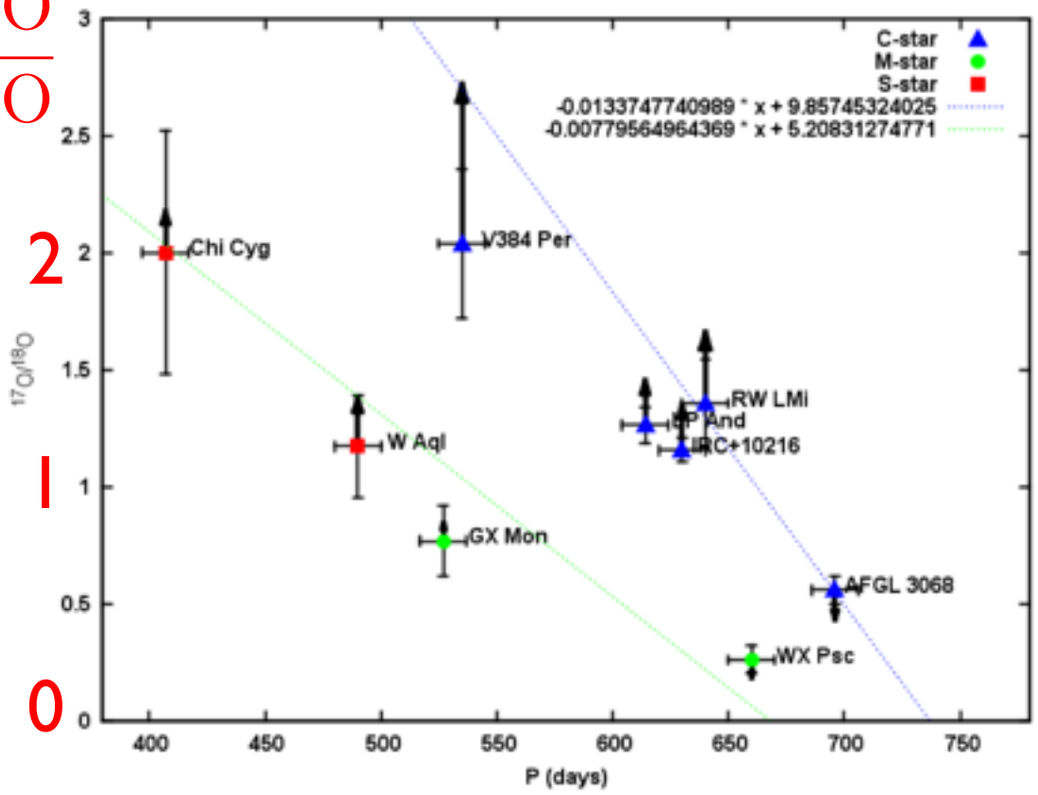

deNutte et al. (in prep)

9 AGB stars with both C^{17}O and C^{18}O

+ some objects with only C^{18}O

Studies of this type are reaching their limits on single telescopes !!

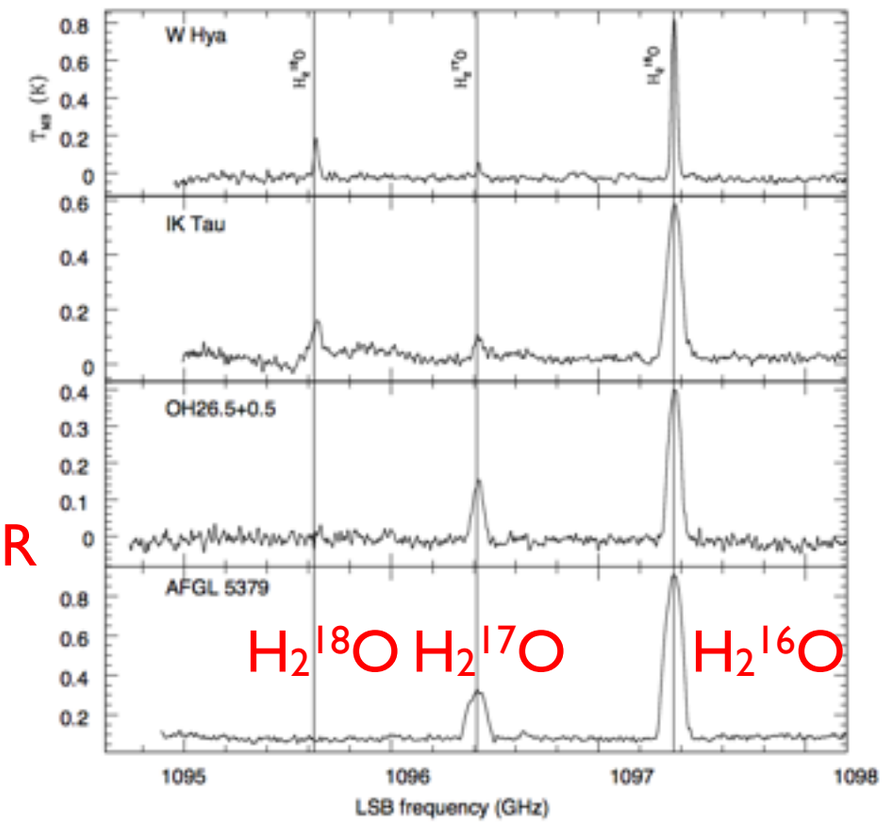

OH/IR

Justtanont et al. (A&A 578, A115, 2015)

9 OH/IR stars with only $H_2^{17}O$ detected

In general, $I(H_2^{18}O)/I(H_2^{17}O) < 0.1$

These are massive stars, $>5M_\odot$

Circumstellar ^{28}Si, ^{29}Si, and ^{30}Si

Peng et al. (A&A 559, L8, 2013):

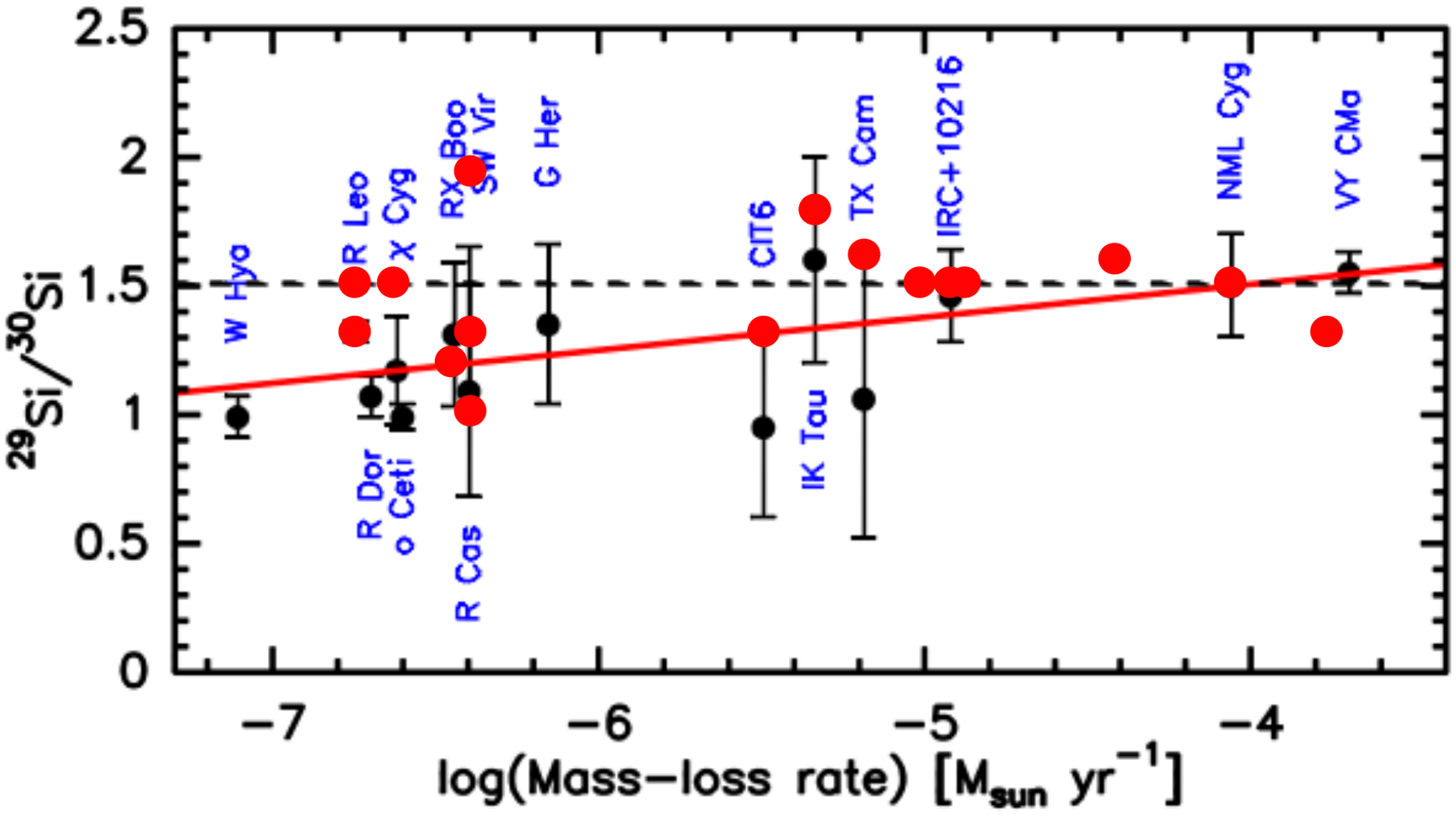

Fig. 2. Comparison of ^{29}Si/^{30}Si in evolved stars. The dashed line indicates the terrestrial and solar ^{29}Si/^{30}Si abundance ratio of 1.51 (de Bièvre et al. 1984; Anders & Grevesse 1989; Asplund et al. 2009). The red line is a linear fit to the ^{29}Si/^{30}Si–$\dot{M}$ relation.

●

New data from OSO 20m telescope.

All three isotopes observed simultaneously and high S/N

Multi-isotope studies

CW Leo

Table 1: Isotope ratios in the CSE of IRC+10216

Isotope ratio	Ratio	IRC/Solar	Species used
$^{12}C/^{13}C$	45	0.5	CS
$^{12}C/^{14}C$	> 63000		CO
$^{14}N/^{15}N$	5300	20	HCN
$^{16}O/^{17}O$	840	0.3	CO
$^{16}O/^{18}O$	1300	3	CO
$^{28}Si/^{29}Si$	18	0.9	SiO, SiS
$^{28}Si/^{30}Si$	27	0.9	SiO, SiS
$^{32}S/^{33}S$	110	1	SiS
$^{32}S/^{34}S$	22	1	SiS
$^{32}S/^{36}S$	2700	0.4	CS
$^{35}Cl/^{37}Cl$	3.0	1	AlCl, HCl, NaCl, KCl
$^{24}Mg/^{25}Mg$	8	1	MgNC
$^{24}Mg/^{26}Mg$	7	1	MgNC

CW Leo, RW LMi, AFGL3068

Table 3
Isotopic Abundance Ratios

Isotopic Ratio	CRL 3068		CIT 6[a]	IRC+10216[b]	Solar[c]
	Species	Value			
$^{12}C/^{13}C$	$^{12}C^{34}S/^{13}C^{32}S$	29.7[d]	45.4	45	89
	$^{12}CO/^{13}CO$	5.6[e]	...	...	...
	$^{12}CS/^{13}CS$	9.8[e]	...	...	...
	$H^{12}CN/H^{13}CN$	1.2[e]	...	...	...
$^{14}N/^{15}N$	$H^{13}C^{14}N/H^{12}C^{15}N$	1099[f]	...	...	272
	$HC^{14}N/HC^{15}N$	45[e]	...	...	...
$^{16}O/^{17}O$	$^{13}C^{16}O/^{12}C^{17}O$	668:[f]	890	967	2680
	$C^{16}O/C^{17}O$	125:[e]	...	...	...
$^{16}O/^{18}O$	$^{13}C^{16}O/^{12}C^{18}O$	472[f]	...	1172	499
	$C^{16}O/C^{18}O$	88[e]	...	...	...
$^{17}O/^{18}O$	$C^{17}O/C^{18}O$	0.7:	...	1.14	0.2
$^{32}S/^{34}S$	$C^{32}S/C^{34}S$	7.4[e]	6.7[e]	18.9	22.5
$^{33}S/^{34}S$	$C^{33}S/C^{34}S$	0.3:	0.2:	0.19	0.18
$^{29}Si/^{30}Si$	$^{29}SiS/^{30}SiS$	2.5	1.0	1.46	1.52
$^{28}Si/^{30}Si$	$^{28}SiS/^{30}SiS$	28.8	8.8[e]	24.7	29.9
$^{28}Si/^{29}Si$	$^{28}SiS/^{29}SiS$	11.5	8.9[e]	17.2	19.6

Notes.
[a] From Zhang et al. (2009).
[b] From He et al. (2008) except the $^{12}C/^{13}C$ ratio which was taken from Cernicharo et al. (2000).
[c] From Lodders (2003).
[d] Assume that the $^{34}S/^{32}S$ ratio is solar.
[e] Should be treated as lower limits due to opacity effect.
[f] Adopted: $^{12}C/^{13}C = 29.7$.

Zhang et al. (ApJ 700, 1262, 2009)

Mass loss

Mass-loss-rate determinations

Mass-loss rates from Ramstedt et al. (2009) and references therin:

These studies are still unique in terms of number of sources.

CO data towards 73 M-stars, 40 S-stars, and 61 C-stars

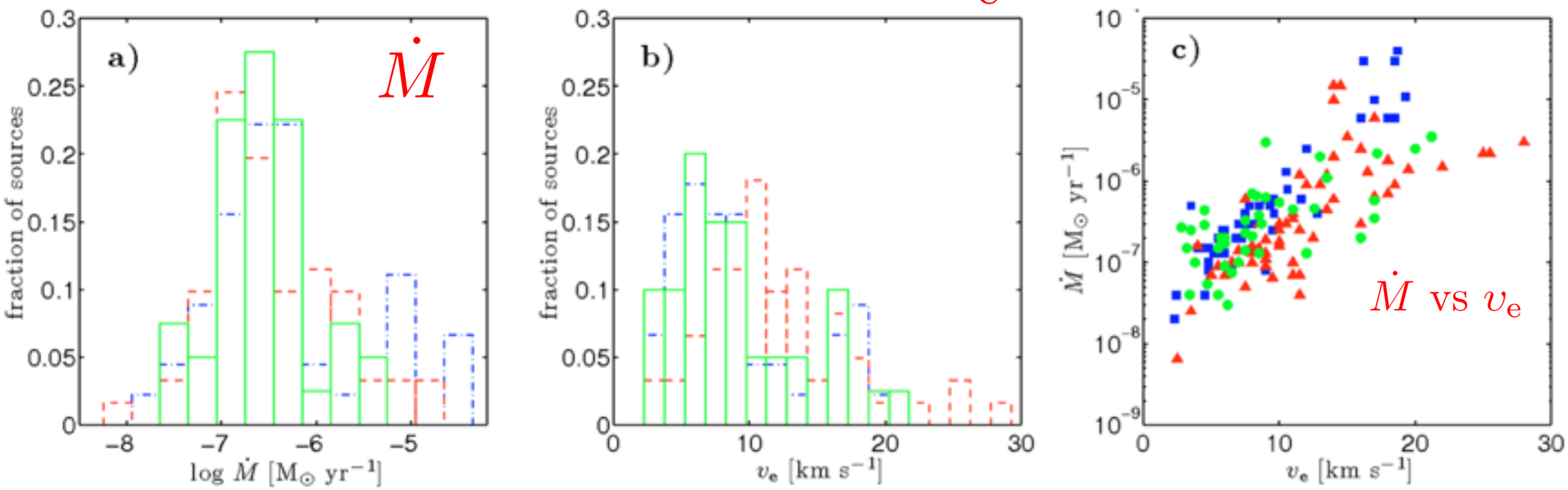

Important constraints on any viable mass-loss mechanism !!

Important to complement with similar studies in different environments, e.g., metallicity !! This needs ALMA !!

See also De Beck et al. (A&A 523, A18, 2010)

Danilovich et al. (in press) derived mass-loss rates for a sample of 40 stars where HIFI CO(5-4, 9-8) data exist (SUCCESS project)

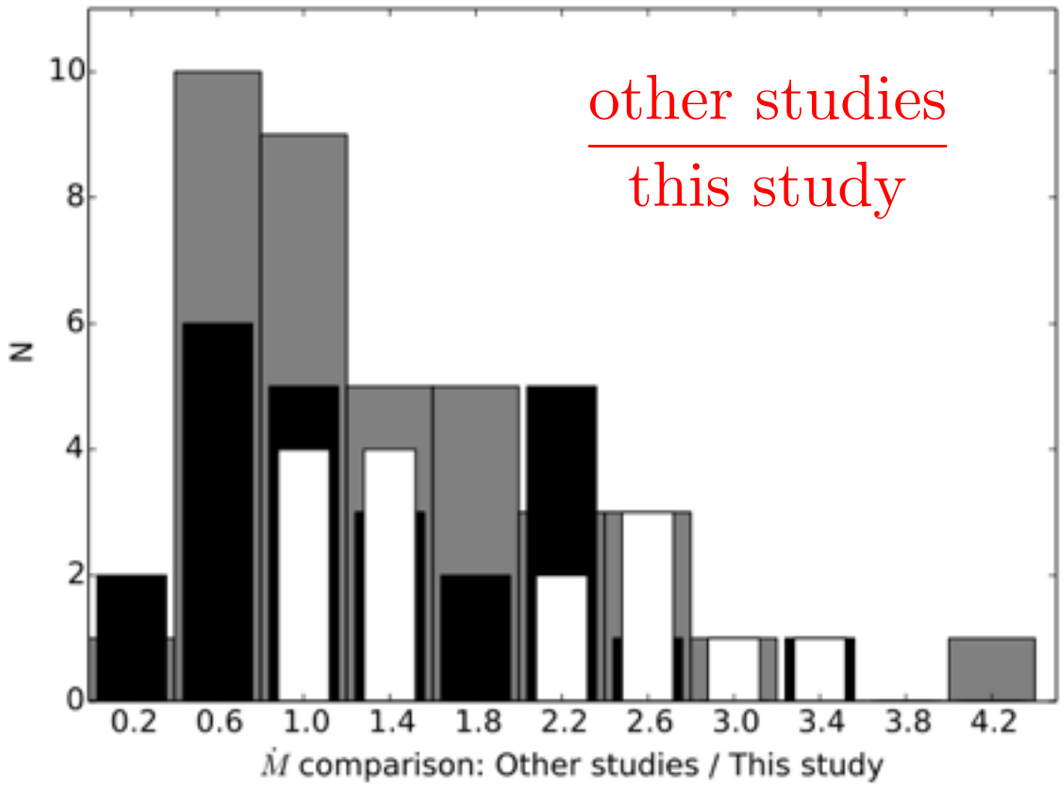

Fig. 7. Comparisons with mass-loss rates from past studies: $\dot{M}_{previous}/\dot{M}_{new}$, grouped by chemical type. C stars are grey, M stars are black and S stars are white.

Mass-loss rates on average 40% lower than previous studies (even after correcting for distances and and CO abundance assumptions).

The spread in the estimates between the studies is about ±50%.

Within the adopted circumstellar models the mass-loss-rate estimates are accurate to within ±50% !!

Is there a superwind?

Justtanont et al. (A&A 556, A101, 2013):

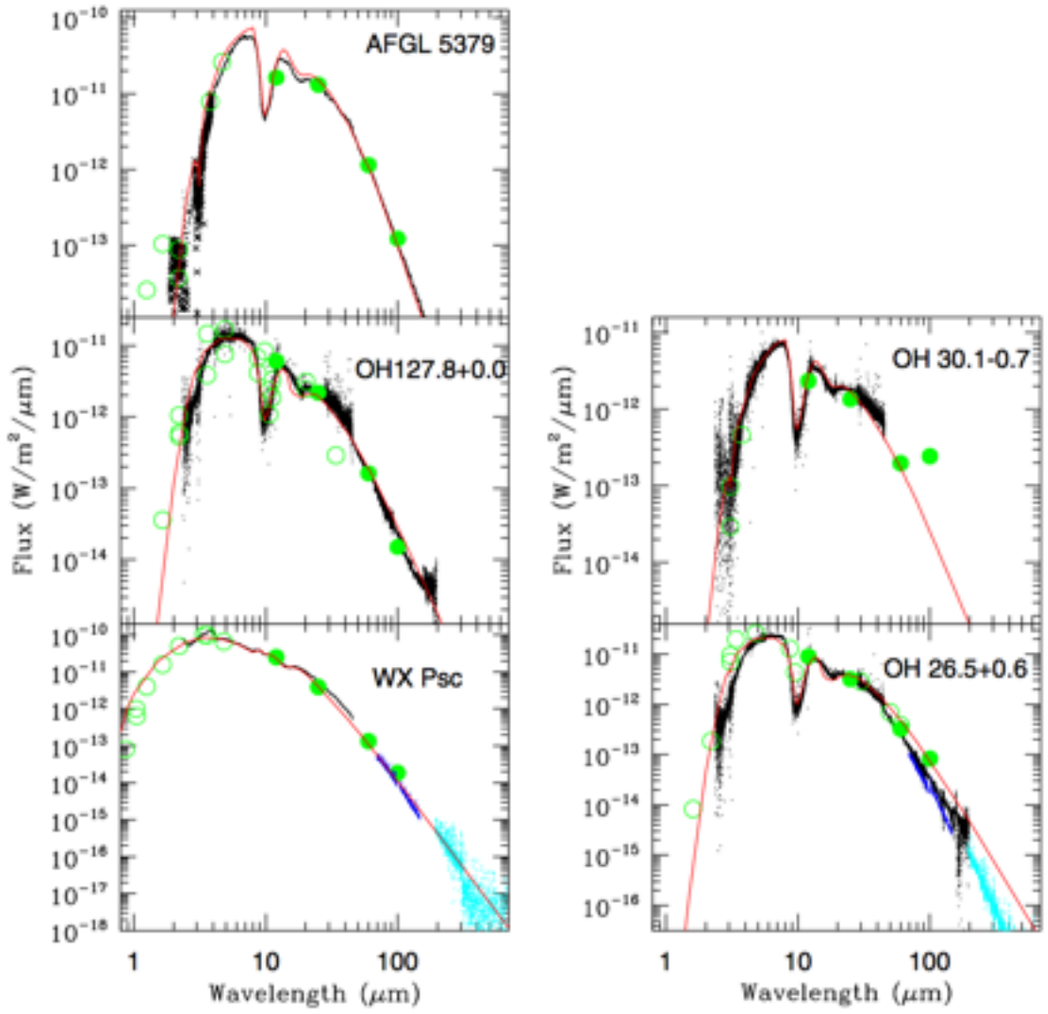

Fig. 1. SED fits for the sample stars (solid line) to the ISO spectra (black dots) and photometric points from IRAS (filled green circles). The PACS (blue dots) and SPIRE (cyan dots) spectra are also plotted when available. The published photometric data (open circles) are taken from Dyck et al. (1974) and Epchtein et al. (1980) for WX Psc, Persi et al. (1990) for OH 127.8+0.0, Garcia-Lario et al. (1997) and Lepine et al. (1995) for AFGL 5379, Werner et al. (1980) for OH 26.5+0.6, and Justtanont et al. (2006) for both OH 26.5+0.6 and OH 30.1-0.7.

4 extreme OH/IR-stars:

$$\dot{M}_{\rm dyn} \approx (2-10) \times 10^{-4}\ {\rm M}_\odot\,{\rm yr}^{-1}$$

$$\dot{M} \approx 3 \times 10^{-6}\ {\rm M}_\odot\,{\rm yr}^{-1}$$

beyond (1-3)x10^{16} cm to explain the low-J CO lines.

With $v_e \approx 15$ km/s this corresponds to a time scale of ≈200 – 600 yr for the SW phase

The amount of mass lost during the SW is of the order 0.1 $M_\odot$!!

de Vries et al. (A&A 561, A75, 2014):
used the 69 μm feature to estimate that the outer radius of the SW must be < 3×10^{16}cm.

Thus, the same problem arises, far too little mass is lost during one SW for the more massive OH/IR-stars !!

Are there several SW phases for an individual star?

What do the OH data tell us about the duration of the SW phase?

Measure the duration using ALMA and CO lines!

$$\int_{t_{\mathrm{AGB}}} \dot{M}(t)\,\mathrm{d}t$$

M_{lost} & large-scale structure

$$\dot{M}(t, \theta, \phi)$$

Conclusions so far from NRT survey of ≈100 stars of different chemical types, variability types, and mass-loss rates in the HI 21cm line (Gerard, Le Bertre, Libert, et al.):

- High detection rates for low mass-loss rates ($<10^{-7}$ $M_\odot$/yr; irregulars and semi-regulars), but lower for Miras
- Double-component line profiles: suggesting an expanding, decelerated wind, and a quasi-stationary shell of material that accumulates between the termination shock and the ISM
- Total HI masses are only of the order few x (10^{-3} - 10^{-2}) $M_\odot$
- HI line centroids are often displaced towards zero velocity (in LSR scale)

Conclusions from imaging of about a dozen sources in HI 21cm line (Matthews et al.):

- Confirm that the HI envelopes are characterised by both its inherent properties and its interaction with the ISM
- Deceleration of the gas is measured; this gives an age estimate of the mass-losing history of the star

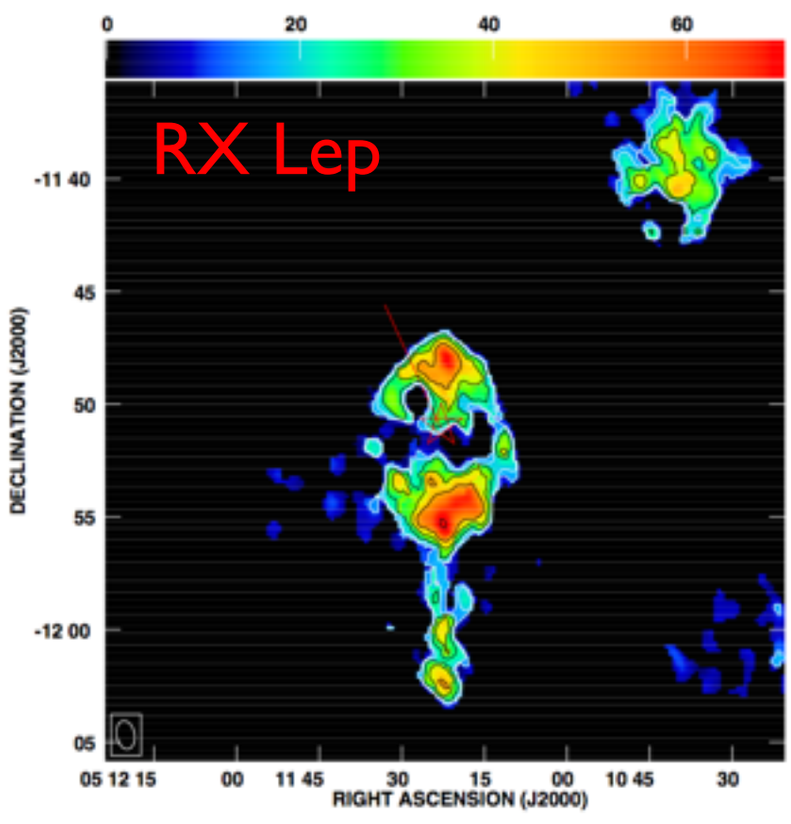

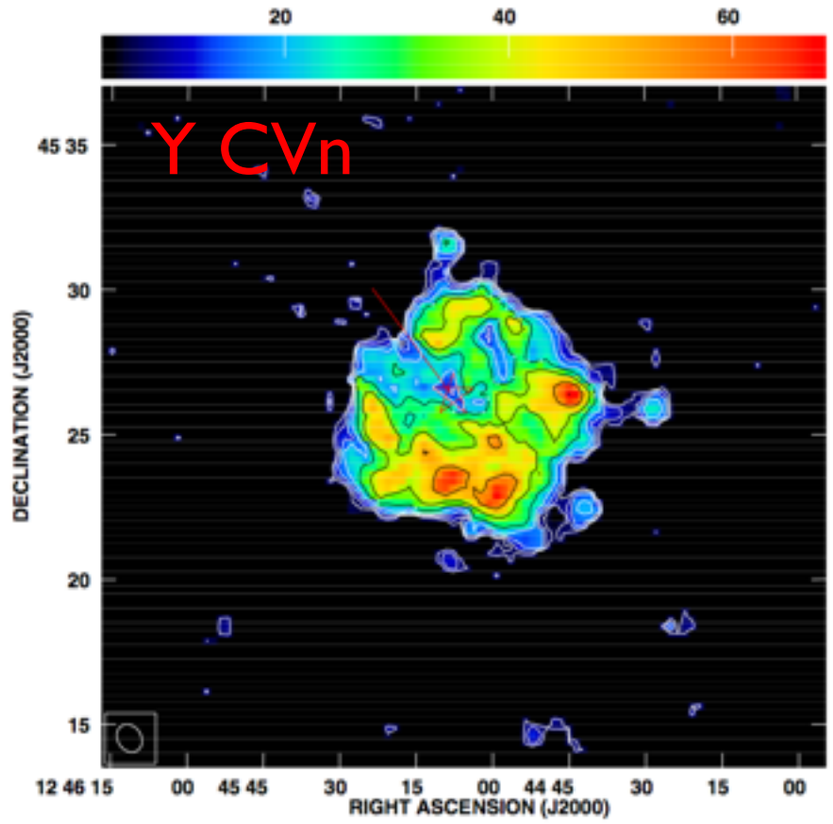

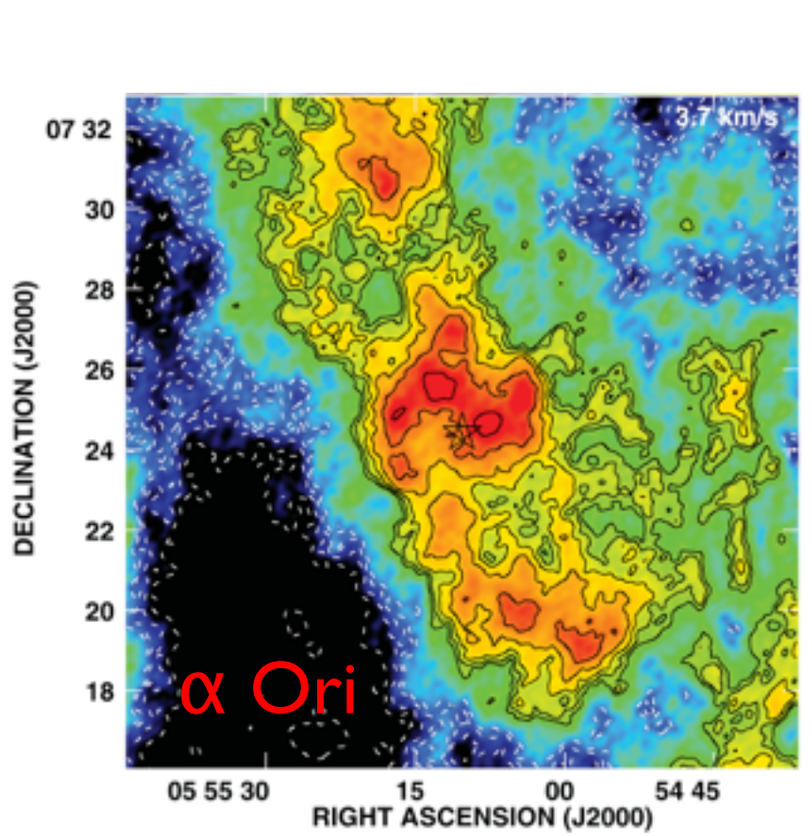

α Ori has been losing matter at a rate of 1.2×10^{-6} $M_\odot$/yr for the past 8×10^{4} yr

Polarisation

There is great hope on what ALMA can do when it comes to polarisation (masing as well as non-masing lines).

Important characteristics:

- Magnetic field strength vs r
- Magnetic field shape
- Origin of magnetic field
- Importance of binarity
- Importance for mass-loss characteristics

Leal-Ferreira et al. (2013)

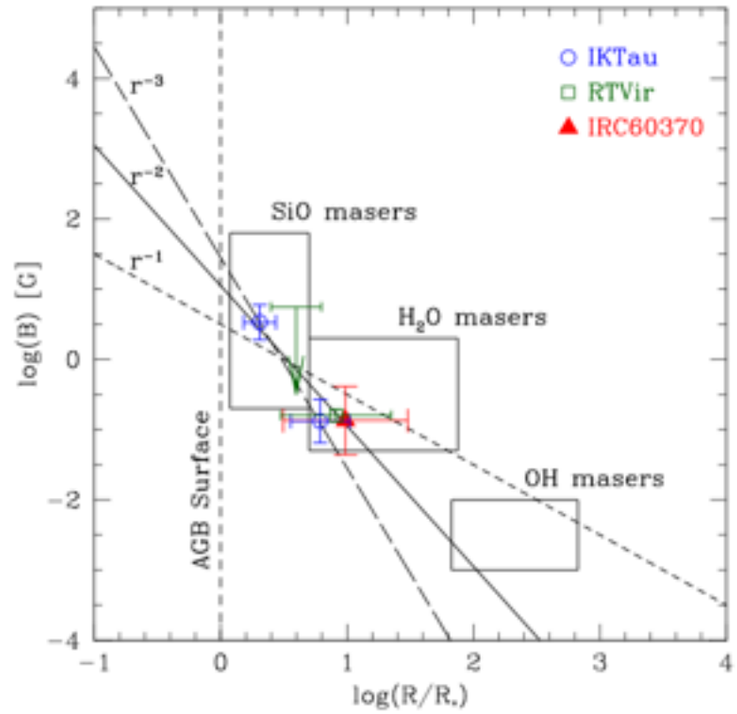

Fig. 5. Magnetic field strength along the line of sight versus the radial distance of the masers to the star. The black boxes show typical regions of the plot where results from the literature for SiO, H_2O, and OH maser occur, and they are normalized for $R_* = 1$ (Vlemmings et al. 2002, 2005; Herpin et al. 2006; Rudnitski et al. 2010). Our measurements are shown by the hollow blue circles (IK Tau), hollow green squares (RT Vir), and filled red triangles (IRC+60370). The short-dashed, solid, and long-dashed inclined lines show a dependence $\propto R^{-1}$, $\propto R^{-2}$, and $\propto R^{-3}$ for the magnetic field, respectively. The position of the AGB surface of a star with radius of 1 AU is also shown.

Binarity

There is great hope on what ALMA can do when it comes to binarity.

CW Leo, CO(2-1)
Cernicharo et al. (2015)

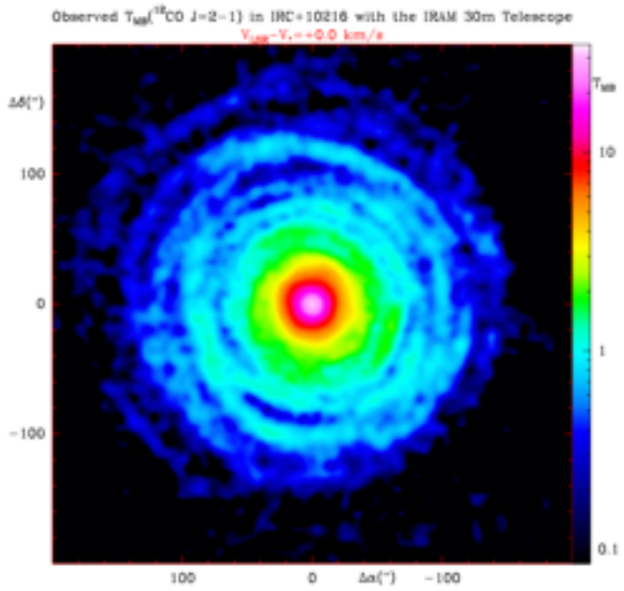

R Scl, CO(3-2)
Maercker et al. (2012)

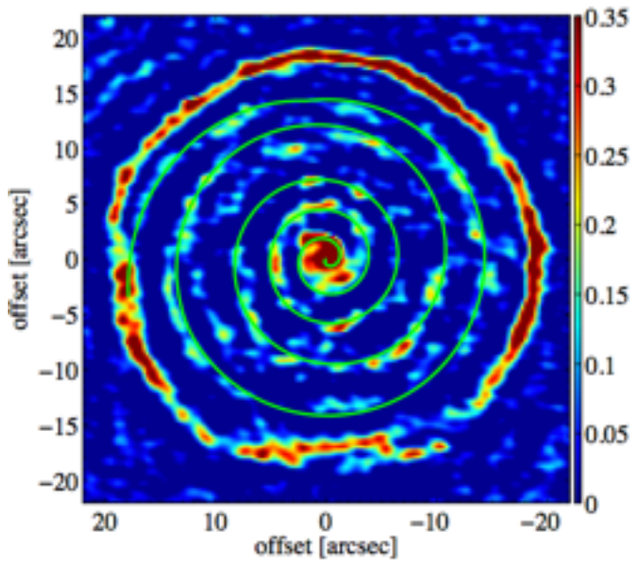

CW Leo, ^{13}CO(6-5)
Decin et al. (2015)

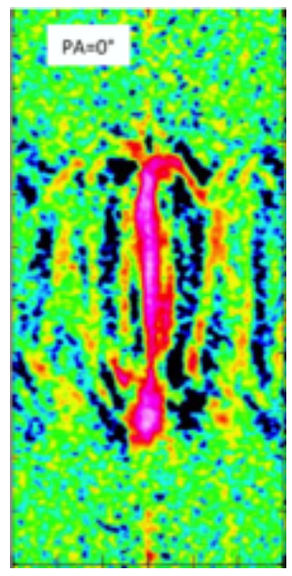

o Ceti, CO(3-2)
Ramstedt et al. (2014)

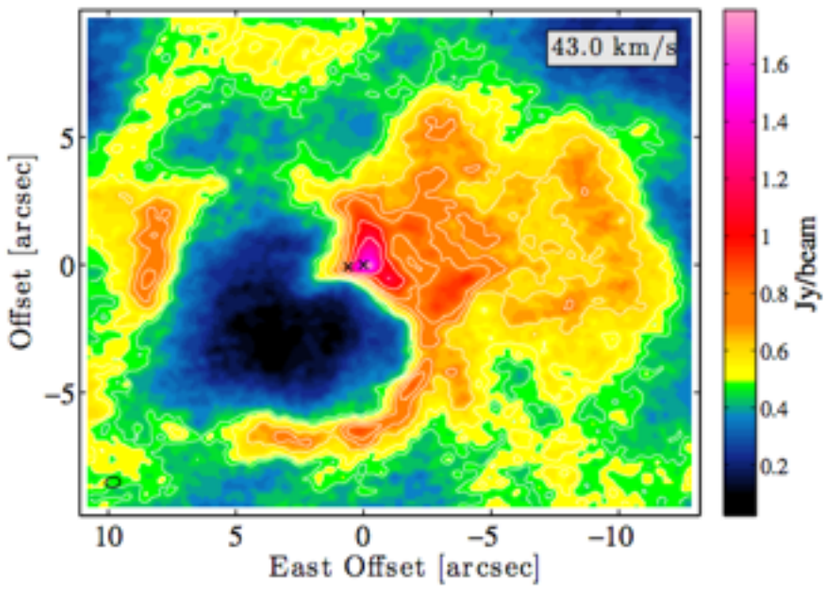

RW LMi, HC_3N(4-3)
Claussen et al. (2011)

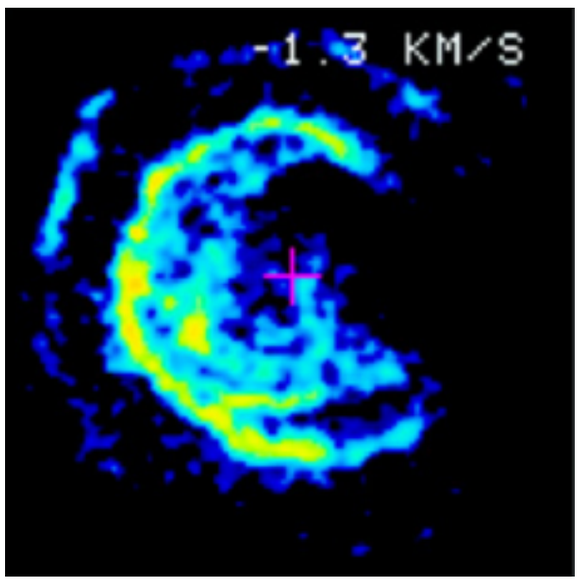

RW LMi, HC_3N(5-4)
Trung & Lim (2009)

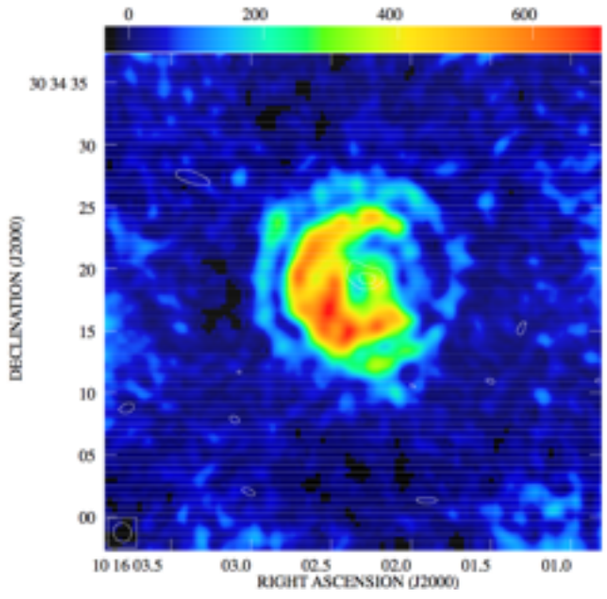

Thank you !!